Pseudo-Three-Dimensional Micropost Array Detector Systems

A THESIS SUBMITTED TO THE FACULTY OF THE UNVIERSTIY OF MINNESOTA BY

Jeffrey David Hyypio

IN PARTIAL FULFILLMENT OF THE REQUIERMENTS FOR THE DEGREE OF MASTER OF SCIENCE

Dr. Patrick Alford, Advisor

May 2021

Acknowledgments

Throughout this thesis project I have received a tremendous amount of support and patience. I would like to thank the Eric Hald, Kerrianne Steucke, and Zaw Win for their assistance acquainting me with countless techniques and equipment including, but not limited to, photolithography, microcontact printing, and cell culturing, all of which were used extensively.

I would be remiss not to acknowledge a critical meeting with Dr. Paul Kimani who shared with me his wisdom and experience in creating and oftentimes salvaging micropillar arrays which proved crucial to any measure of success early on in this project.

Of course I am beyond obliged to thank my advisor, Dr. Patrick Alford, who has to varying degrees (the balance of which I hope to never learn) both tolerated and encouraged my perseverance with this project, even when life beckoned me to step away from it entirely.

And if I am allowed one more acknowledgment, I will use it to thank my wife, Emily, who may be the only person more delighted than I am to have finally completed this undertaking.

Abstract

In this project, a novel pseudo-three-dimensional micropost array detector system (mPADs) was fabricated with the intent of understanding its utility for observing and modulating cellular motility in a 3D environment. For over a decade, traditional mPADs have been manufactured from polydimethylsiloxane (PDMS) and used to isolate substrate rigidity as the dependent variable in single cell experiments. This work recounts the design and fabrication process required to construct the final device which consists of an upward-facing bottom mPADs layer, a downward-facing top mPADs layer, and a spacing layer of controlled thickness separating them and allowing cells to migrate on by adhering to the protein-functionalized surfaces of each mPADs simultaneously. Several devices were successfully fabricated and seeded with human umbilical artery smooth muscle cells (HUASMCs), however there were no confirmed events where a cell simultaneously adhered to both the top and bottom mPADs device at the same time.

Table of Contents

List of Figures

List of Tables

1 Introduction

1.1 Motivation

Cell migration is a fundamental process which determines tissue development, wound healing, disease, and homeostasis (Ridley, 2003). One such process of particular interest is restenosis of vascular tissue following disease or trauma. Heart disease kills approximately 650,000 Americans annually (Virani et al., 2020), and the market for medical devices intended to treat cardiovascular disease is expected to reach nearly $70 billion by the year 2026 (Data, 2019). Smooth muscle cell recruitment and migration to damaged vascular tissue is critical for restenosis (Faxon et al., 1997). Consequently, SMC migration occurring in excess is a major complicating factor in the placement and long-term use of cardiovascular devices, such as angioplasty or coronary stent placement (Merkle et al., 2015). Traditional assays of cell migration observe the behavior of cells spread onto a two-dimensional surfaces (e.g. scratch-wound assay, cell scatter assay, etc.) (Wells, 2011). The goal of this research is to create a novel tool for understanding cellular motility in a non-spread, pseudo-three-dimensional state. The methods laid out below can replicated with a basic understanding of photolithography and cell culture. A pseudo-3D mPADs device could be inexpensively replicated and applied to a host of cellular studies.

1.2 Background

1.2.1 Cell Migration

As described above, injuries to tissue structure can prompt SMC migration. Locomotion of individual eukaryotic cells (including SMCs) often begins with the formation of a pseudopod at the leading edge; crosslinked networks of actin filaments rapidly polymerize in the direction of the leading edge and depolymerizing at the trailing edge, pushing the cytoplasm further and further forward (Blanchoin et al., 2014). Adhesion receptors (consisting of surface proteins and integrins) on the psuedopodial extracellular matrix collide with and adhere to the substrate, linking the advancing cytosomal actin network to the substrate (Zaidel-Bar et al., 2007). Once adhered, the movement of the cell can be controlled by regulating the actin network and the degree of adhesion, which itself can be regulated by the cell via modulation of the activity and localized density of adhesion receptors (Pollard et al., 2017). Further polymerization of the anchored actin network results in advancement of the leading edge of the cell, while disintegration from the substrate causes the polymerizing actin network to push itself back toward the center of the cell via *retrograde flow*, in a sense making the cell "spin its wheels" (Pollard et al., 2017).

1.2.2 History of mPADs and their uses

Elastomeric microposts have been used to isolate substrate stiffness as a variable of the extracellular environment since 2003 (Tan et al., 2003). These substrates consisting of a bed of micro-scale polymeric pillars geometrically spaced to allow for the adhesion and quasi-planar deformation of individual cells were coined micofabricated post-array detectors (mPADs). Cells would attach to the top surface of multiple posts and apply

forces, which could be easily computed under the assumption that the posts behaved as vertical cantilevers under pure bending. The posts could be organized in way such that the individual sub-cellular structures could undergo large deformations without significant displacement of the underling sub-post basal layer (Zhao et al., 2005).

The design of the mPADs allow for the isolation of substrate stiffness as the only independent variable of the extracellular environment. Previous approaches to studying the effects of cell substrate stiffness also inherently changed the physical or chemical properties of the substrate itself and required tedious calculation to extract quantitative data.

One method first used by Harris et al in 1980 involved fabricating silicone films which were sufficiently thin such that applied forces by adherent cells induced wrinkles in the film, in so demonstrating that cells in vivo could generate significant planar tension underneath the cell itself, not only at the edges of the cell (Harris et al., 1980). While this method was able to approximate an absolute magnitude of shear forces, deriving more localized cellular forces, however, becomes much more difficult in this apparatus and would involve complex geometry and failure mechanics.

The fidelity of localized cellular force generation was improved when Traction Force Microscopy (TFM) started being utilized in the 1990s to measure the displacement of fluorescent beads impregnated near the surface of elastomeric gel. Cells cultured on thin synthetic polyacrylamide (PAA) gels coated in collagen demonstrated stronger transient forces on the leading edge of a migrating cell and weaker forces in the posterior areas of the cell (Pelham and Wang, 1999). The synthetic gels were linearly elastic with

bulk properties were easily defined using Young's modulus. Still, later study of the synthetic polymers as cellular substrates demonstrated that changes in surface properties such as wettability and roughness could affect cell behavior as well as changes in bulk elasticity (Ying Mei et al., 2010). Therefore, if the bulk properties of a synthetic polymer is altered, the surface properties of the substrate must also be accounted for.

Alternative approaches utilized naturally-occurring extracellular matrix proteins and polysaccharides to form gels. By chemically cross-linking biopolymer networks, the gels can form either two- or three-dimensional networks with functionally similar behavior as *in vivo* cellular environments. Extracellular matrix proteins have been shown to interact with numerous growth factors and have an important function in controlling cellular behavior. Fibrin and f-actin networks behave as non-classical rubbers with rubbery plateau moduli that scale with increasing chemical cross-linking of protein monomers (MacKintosh et al., 1995). However, because of the aforementioned growth factor and other protein interactions, not to mention steric hinderance, changing the cross-linking of proteins in the matrix or using protein fibers of different thickness can yield changes in cellular behavior independent from mechanical changes (Georges and Janmey, 2005). Synthetic matrices, such as PAA, have the advantage of being chemically inert and able to be locally functionalized with adhesive ligands.

Galbraith and Sheetz attempt to tease out the cellular traction forces generated during cell migration using micromachined horizontal cantilevers (Galbraith and Sheetz, 1997). The devices were fabricated by photolithographic etching of phosphosilicate glass-on-silicon substrates to create a substrate layer consisting of an array of pads fixed

below the substrate layer to a cantilever (Galbraith and Sheetz, 1998). Cells adhering to the cantilever-fixed pads were able to deflect the pads along the in-plane perpendicular axis, and the localized cellular traction force vectors could be trigonometrically calculated using the cantilever's stiffness (Galbraith and Sheetz, 1997). This apparatus, while clever, requires technical nous to repeat the photolithographic manufacture of devices with varying cantilever stiffness and cell contact pad size. This technological hurdle could limit the mass production of devices for experimental use for users without access to such knowledge or sufficiently precise equipment.

While Tan et al's first generation of micropost arrays consisted of a square array of 3μm posts with center-to-center spacing of 9μm, further studies investigated the effects of varying post geometries and array spatial geometries. Assuming the bulk material properties of the polymer used to construct the mPAD devices are fixed, the post height, cross-section, and spacing can be modified to obtain different substrate rigidities. mPADs with 2μm diameter and 3μm center-to-center spacing were used to successfully map traction forces generated by Madin-Darby canine kidney (MDCK) epithelial cells. Positive or negative masters used to produce batches of finished devices were originally made using traditional photolithography techniques with photoresist selectively exposed to ultraviolet light through a reticle photomask. These could create sufficiently resolved features for many experimental applications and contemporary mPADs can even be fabricated with features as small as 500nm by using deep trench etching or other advanced lithography techniques (Michael T Yang et al., 2011).

1.2.3 Approaching three dimensions

All experimental apparatuses described in section 1.2.1, including mPADs, are only are able to study behavior of cells spread on a two-dimensional surface. While they are still certainly useful in understanding cell behavior, cells on these devices are spread in a manner not often occurring naturally in vivo. Within the natural extracellular matrix, cells will migrate, polarize, and/or self-organize in various fashions depending on the cell function or environment (Schwartz and Chen, 2013). The free body diagram for a cell in 2D is dominated by shear stresses, where in a 3D environment the cell can exert both shear and normal principal stresses. Modifying the traditional mPADs structure to introduce a perpendicular strain component would allow for new practical study of cell behavior in 3D while maintaining the aforementioned ability of mPADs to isolate substrate stiffness as an independent variable.

3D cellular behavior is of particular interest in the study of cell invasion and invagination. Migrating cells in vivo are required to navigate a complex 3D geometry. It has already been shown that 3D experimental apparatuses more closely reflect *in vivo* tissues compared traditional 2D set-ups (Elliott and Yuan, 2011). Independent of proteolytic factors, cell migration can be affected by

The process of cell adhesion and motility in the 3D has been the subject of some dispute, though more recent research downplays the fundamental difference in behavior in 2D and 3D environments. The concept of a "focal adhesion" was first introduced by Abercrombie et al in 1971, who noted that only one quarter of the surface area of migrating fibroblasts was adjacent to their 2D substrate in localized "electron-dense

plaques containing longitudinal filaments" (Abercrombie et al., 1971). Important adhesion proteins, such as vinculin and integrin, and/or cell-matrix adhesions have been observed in 3D systems in fibroblasts, smooth muscle cells, carcinoma cells, and endothelial cells (Cukierman et al., 2001; Li et al., 2002; Wozniak et al., 2003; Zhou et al., 2008).

Interestingly, in 2010 Fraley et al found that when fibrosarcoma cells were sandwiched between a collagen-coated hard basal and a thick collagen apical gel in a pseudo-3D apparatus, the focal adhesion size and quantity was significantly reduced compared to the collagen-coated basal surface alone (2D), and the cells did not produce any focal adhesions on the top layer (Fraley et al., 2010). Furthermore, the investigators were unable to detect any focal adhesion structures in cells fully immersed in collagen in a true 3D extracellular matrix, concluding that if said structures exist they would be less than 0.3 μm and remain stable for less than 1s. The following year, however, a study by Kubow and Horwitz found that by decreasing sources of background fluorescence, discrete focal adhesions could be imaged on the leading edge of the protrusions of cells migrating in a 3D collagen matrix and suggested that certain microenvironmental factors may influence the formation and regulation of adhesion complexes(Kristopher E. Kubow and Alan Rick Horwitz, 2010). Moreover in 2012, Tolde et al conducted scanning electron microscopy of sarcoma cells in a complex 3D collagen matrix of varying fiber thickness and revealed that similarly sized focal adhesions were found in the 3D matrix as in 2D conditions (Tolde et al., 2012). This study proposed differences in cellular behavior when in a homologous network of thin filaments, as in the reconstituted

collagen gels used in the Kubow and Horwitz study versus the varied fibrillar nature of native gels, with fiber thickness ranging from 0.1 to 8 μm. Focal adhesions large enough to facilitate cell migration may require sufficiently large fibers (Tolde et al., 2012).

2 Method

2.1 Master Wafer Fabrication

The process for creating a master wafer from which individual mPADs devices could be fabricated was largely based on the method used by Sniadecki and Chen in 2007 (Sniadecki and Chen, 2007). SU-8 (MicroChem, Inc., Newton, MA) is a commonly-used photoresist and had already been successfully used to create other devices in the Alford lab.

2.1.1 Design and fabrication of the reticle photomask

Design of the photomask was driven by multiple factors. Due to the cost of production, combined with the inexperience with photolithography, it was decided that one mask would be used to create molds of different post stiffnesses. The 4-inch diameter wafer could accommodate several individual device molds. The goal was to ultimately create mPADs with varied post stiffnesses. Assuming each post is a slender cylindrical beam of uniform thickness, the force, F required to deflect a post top by distance, x can be calculated by,

(1) $$F = \left(\frac{3\pi E D^4}{64 L^3}\right) x$$

.

Assuming a constant elastic modulus, *E*, post diameter, *D*, and post length, *L*, the post stiffness can be interpreted as an effective spring constant, *k* consisting of the part of equation (1) in parentheses.

(2) $$k = \frac{3\pi E D^4}{64 L^3}$$

The elastic modulus could be changed in fabricated devices by changing the ratio of PDMS base to curing agent or changing the curing time. However, the tall, thin features of mPADs are already prone to collapse during fabrication and functionalization and a consistent higher modulus material would be preferred, structurally (Amato et al., 2012). Changing the length of the beam could be accomplished by either creating multiple master silicon wafers using different thicknesses and exposure times or making multiple reticle photomasks to which could be sequentially aligned to create discrete devices on one wafer with different feature heights. This would be ideal, as the functionalized area of the microposts would remain unchanged with varied post stiffness, but also requires additional process steps. Finally, the diameter of the posts could be varied to impose a fourth-power change in post stiffness. One reticle photomask could be used to create devices with varying post diameters. This requires only one successful mask fabrication and did not rely on multiple mask alignment.

The feature height/width ratio using contact photolithography is limited by the wavelength of light being used. The theoretical post diameter, D, for a post of height, H, at photoresist absorption wavelength, λ, is given by

$$D = \frac{3}{2}\sqrt{\frac{\lambda H}{2}} \quad (3)$$ (Madou, 2002).

Therefore, when using 10 μm thick SU-8 photoresist, which is optimized for 350-400 nm exposure, the theoretical obtainable diameter is approximately 2.0 – 2.1 μm. A 2:1 ratio of the post-post distance to the post diameter ("single spacing") was chosen as it was shown to isolate the cell from the underlying post substrate while providing enough space for post top movement (Zhao et al., 2005). Larger center-to-center spacings have been shown to inhibit cell spreading and migration (Michael T Yang et al., 2011). Using constant micropost height, four cylindrical post diameters were chosen to obtain over a nine-fold range in post stiffness.

Table 1: Comparative stiffness of chosen micropost diameters*

Post Diameter (μm)	**Center-Center Spacing (μm)**	**Stiffness, *k***
2.0	4.0	k_0
2.5	5.0	2.44 k_0
3.0	6.0	5.06 k_0
3.5	7.0	9.38 k_0

*Note: As the actual stiffness, *k* (equation 2) is a function of both the post height and the material elasticity, which for PDMS is itself a function of the base-to-curing agent ratio and bake time, the

stiffnesses are presented only in comparison to the stiffness of a 2.0 μm of equal height. This reference stiffness is denoted as k_0.

As for the macro-structure of the devices, each device would need to support the weight of one or more contact printing stamps, plus contain enough surface on the perimeter to adhere to a spacer layer to prevent direct contact of the features of the confronting mPADs.

Although many reticle photomasks for use in photolithography can be made inexpensively by printing the mask features on an acetate transparency film, high resolution printers would only be able to provide 10 μm features at best. (Sniadecki and Chen, 2007) Instead a chrome on soda lime glass photomask was ordered from the Minnesota Nano Center, which is capable of producing circular features as small as 1.5 μm.

The photomask layout was designed using ICED™ Version 4.88 (IC Editors, Inc., West Linn, OR, USA). Below is a representative schematic of the reticle photomask pattern for an individual mPADs (Figure 1) as well as the 4 × 4 layout of all 16 devices on the soda lime photomask (Figure 2). Each device has a 2.5 mm-wide perimeter wall, four 5 × 5 mm regions of single-spaced posts, and four 4 × 2 mm supporting partitions dividing the post regions into quadrants. The thick perimeter wall and partitions were the same height as the top of the posts and would be used to support the weight and application pressure of a flat stamp without collapsing the delicate microposts. (Note: There is also a 4 × 4 mm square area in the center of the device as well as four 1 × 1 mm

square areas in the outer corners of each micropost field without any features and only basal layer. In early planning of the photomask, it was thought that featureless voids would be useful for creating injection/drain sites, but this feature was later deemed unnecessary and was never realized.)

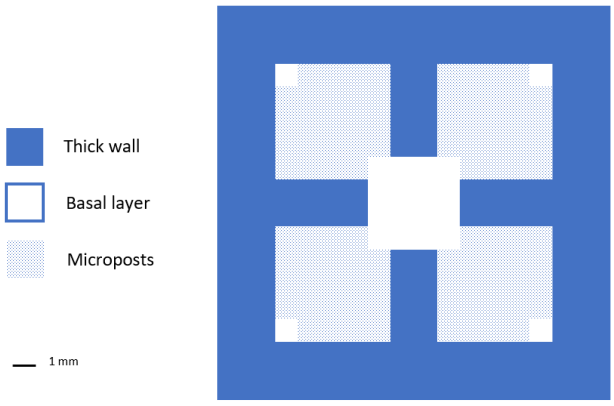

Figure 1: Individual mPADs reticle photomask design

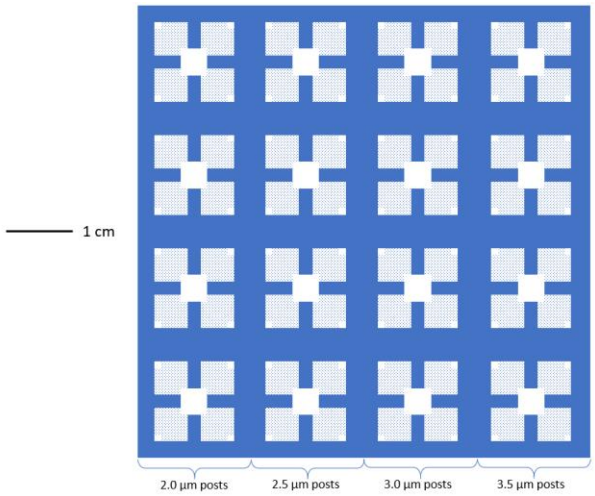

Figure 2: Full reticle photomask design

The ICED file was sent to the Minnesota Nano Center who then fabricated the chrome on soda lime glass reticle photomask.

2.1.2 Fabrication of the master wafer.

The actual master wafer was also manufactured using equipment at the Minnesota Nano Center. A silicon wafer was prepared by immersing sequentially in acetone, methanol, and isopropanol baths for 60 seconds and then quickly drying it with nitrogen gas. The wafer was then dehydrated for 30 minutes on a hot plate preheated to 175 °C. Finally, the wafer was cleaned in a Model 42 Series UVO-Cleaner (Jelight Company, Inc., Irvine, CA) for 10 minutes, followed by a deionized (DI) water rinse and quick dry with nitrogen gas.

The cleaned wafer was then loaded onto a Cee® Model 100 spinner (Cost Effective Equipment, LLC., Rolla, MO). SU-8 2002 photoresist (MicroChem Corp, Westborough, MA, USA) was dispensed onto the center of the wafer to form a circular puddle approximately 1/3 the diameter of the wafer itself (approximately 4 mL) to form the basal layer onto which the posts would later be added. The spinner was set to spin at 500 rpm for 5 seconds at an acceleration of 100 rpm/second, followed by 2000 rpm for 30 seconds with an acceleration of 300 rpm/second. Sniadecki and Chen then performed a soft bake routine of placing the wafer on a 65 °C hot plate for 1 minute and then a 95 °C hot plate for 2 minutes to dry the solvent out of the film, but rapid temperature changes can lead to cracking of the SU-8 material and, later in the process, collapse of the micropost array (Amato et al., 2012), (Li et al., 2016). Instead, the following post exposure bake routine in Table 2 was used at the suggestion of MNC Assistant Scientist, Paul Kimani and adapted from Li et al, 2016. The Model HP131725 Super-Nuova hot plates (Thermo Fisher Scientific Inc, Waltham, MA, USA) used in this procedure did not have a programmable ramping function to control the rate of heat increase/decrease, but, per device general specifications, take approximately 5 minutes to reach temperature. The wafer was placed on a room temperature hot plate and then the hot plate was turned on and set to the temperatures indicated. Also, the SU-8 layer used here is significantly thinner than that used by Li et al so the bake times and ramp down time to room temperature was significantly reduced compared to the published method.

Table 2: Soft Bake Routine

Step	Temperature	Duration
1	Room to 50 °C	5 min
2	50 °C to 65 °C	5 min
3	65 °C to 95 °C	5 min
4	95 °C to Room	~60 min

Following the soft bake, the wafer was flood exposed with a blank glass reticle photomask to 70 mJ (5.8 seconds at ~12 mWatt/cm^2 over ~81 cm^2 surface) in a MA/BA6 mask aligner (Süss MicroTec SE, Garching, Germany). Then the following post-exposure bake protocol in Table 3 was used, again adapted from Li et al.

Table 3: Post-Exposure Bake Routine

Step	Temperature	Duration
1	Room to 65 °C	5 min
2	65 °C to 85 °C	10 min
3	85 °C to Room	~60 min

To create the micropost array, the wafer was again loaded onto the spinner with approximately 4 mL of SU-8 2010 this time dispensed onto the wafer surface. The spinner was set to spin at 500 rpm for 5 seconds at an acceleration of 100 rpm/second, followed by 4000 rpm for 30 seconds with an acceleration of 300 rpm/second. The same

soft bake routine was used from Table 2. Following the soft bake, the wafer was loaded back into the mask aligner, this time with the MNC-manufactured soda lime mask also loaded and aligned into the machine. The mask aligner was programmed for a soft contact exposure of 80 mJ (6.7 seconds at ~12 mWatt/cm^2 over ~81 cm^2 surface). Then the same post-exposure bake protocol from was used from Table 3.

To develop the photoresist, baths of propylene glycol methyl ether acetate (PGMEA) (×2), isopropyl alcohol, and hexane (×2) were prepared, with the development routine described in Table 4. Typically, un-exposed SU-8 photoresist is washed with only isopropyl alcohol, but given the small feature size and fragility of the post structures, hexane, a solvent with lower surface tension, was used for the final baths in development.

Table 4: Development routine

Step	Bath	Duration
1	PGMEA bath 1	2 minutes
2	PGMEA bath 2	5 seconds
3	Isopropyl Alcohol	20 seconds
4	Hexane bath 1	5 seconds
5	Hexane bath 2	5 seconds

The wafer was then hard baked for 24 hours on a 150 °C hot plate. The wafer was then transferred from the clean room to the Nils Hasselmo Hall lab space for the final step of silanization. The wafer was left overnight in a vacuum desiccator with

approximately four drops of trichloro (1H, 1H, 2H, 2H-perfluorooctyl) silane (Sigma Aldrich) placed in a separate dish in in the chamber. Figure 3 shows the fabricated wafer.

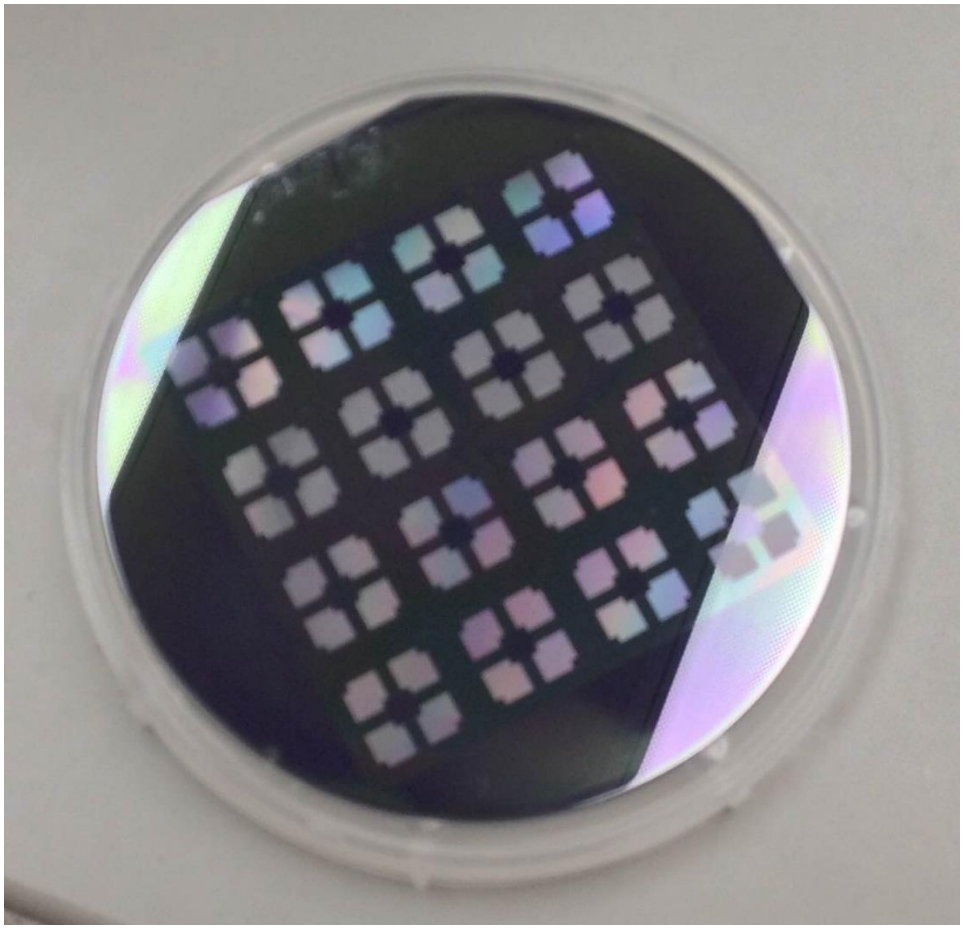

Figure 3: Fabricated mPADs mold on silicon wafer

2.2 Fabrication of mPADs

2.2.1 Creating negative mPADs molds

The fabrication procedure for individual mPADs devices was adopted from Yang et al's 2011 protocol.(Michael T Yang et al., 2011) The silanized wafer was placed in a

clean 6-inch petri dish. Sylgard 184 Polydimethylsiloxane (PDMS, Dow, Midland, MI, USA) was prepared by mixing a 10:1 ratio of PDMS base to PDMS curing agent in a Thinky AR-100 planetary centrifugal mixer (Thinky USA, Inc., Laguna Hills, CA, USA) and degassing the mixture for 60 minutes in a vacuum desiccator. The PDMS mixture was then gently, and in one motion, poured onto the wafer in the petri dish. The dish was then covered and placed in a 90 °C oven overnight.

The next day the dish was removed from the oven the PDMS and wafer were carefully sliced out and placed on a clean cutting mat. Any excess PDMS on the back side of the wafer was removed and then the solid PDMS was peeled off the wafer, keeping the back of the wafer firm against the mat. A clean razor was used to dissect the negative cast of the wafer into each individual 17 × 17 mm molds, keeping them organized to identify where each mold was located on the original wafer (Figure 4).

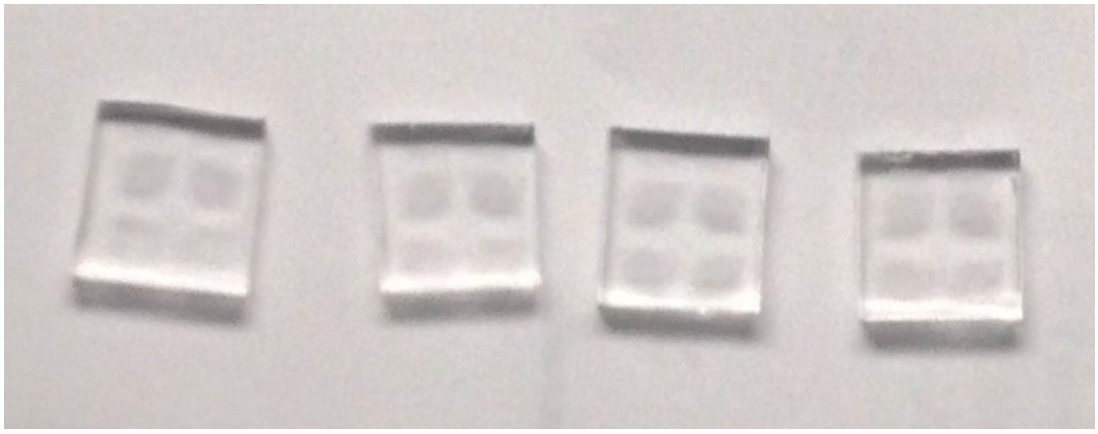

Figure 4: Individual 17 x 17 PDMS mPADs negative molds

2.2.2 Creating PDMS mPADs

2.2.2.1 Preliminary issues

The basic method for creating positive casts of the microfabricated mPADs design is to silanized the negative molds created in section 2.2.1 and to apply fresh PDMS epoxy to the feature surface followed by a bonding platform, such as a glass coverslip. Early attempts at this process, however, did not yield well-formed final devices with defined micropost features.

The first batches were attempted to be created by silanizing the negative molds for 4+ hours, applying a droplet of degassed (30 minutes in vacuum desiccator)10:1 base:cure PDMS to each mold and lightly pressing a 25 mm circle coverslip (Fisherbrand Model 12-545-102, Fischer Scientific, Pittsburgh, PA, USA) onto the uncured PDMS to press out any air bubbles. This model of coverslip was large enough to cover the entire mold surface but was too thin (0.13 to 0.17 mm, per Fisher Scientific specification) and would very frequently fracture when attempting to peel off the mold.

Next, thicker 18 × 18 mm square coverslips (Fisherbrand Model 12-540A) were used in the same manner. This greatly improved coverslip survival during the peel-off step, but the post array was still not well-formed. A fast check to predict if a perfect or near-perfect post array was formed in the PDMS mPADs is to move the array surface slightly under a light source. Well-formed arrays will produce a refraction pattern (Figure 5: Light Refraction Pattern on Well-Formed mPADs) where collapsed posts will look cloudy or translucent (Michael T Yang et al., 2011). This is shown in Figure The Yang et al *Nature Protocols* paper also suggested plasma cleaning prior to silanization to improve

silane adhesion, so the procedure was then modified to include 60 seconds of plasma treatment in a Harrick model PDC-32G (Ithaca, NY, USA) set at “high” power. This step appeared to marginally improve results, but still the posts were largely collapsed, judging both by the light refraction check and after further inspection under microscope.

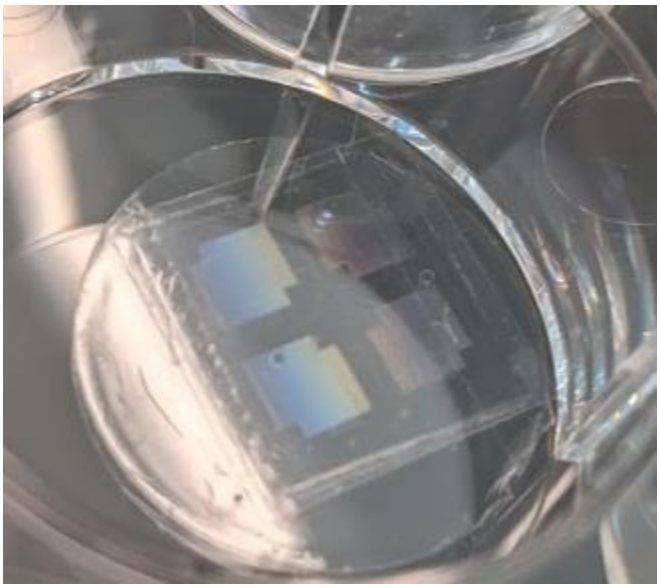

Figure 5: Light Refraction Pattern on Well-Formed mPADs

2.2.2.2 Success with sonication and critical point drying

While the post arrays were largely collapsed, it was clear that many of the posts were still well-formed but had adhered to other posts in small clusters of 3 or 4 posts (Figure 6: Clusters of Collapsed Posts).

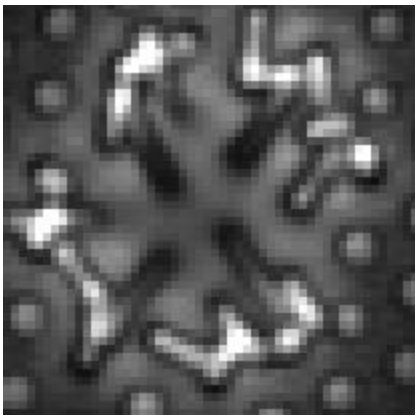

Figure 6: Clusters of Collapsed Posts

The Yang et al *Nature Protocols* paper suggested sonication of posts in ethanol for 1-2 minutes followed by supercritical point drying. The MNC had an Automegasamdri-915B critical point dryer (Tousimis, Rockville, MD, USA). The chamber of the machine, however, had spacer rings to hold 10 × 10 mm square die or 2-, 3, 4-, or 6-inch diameter round wafers, not the 18 × 18 mm square coverslips that were strong enough for device fabrication. Additionally, the device took approximately 90 minutes to operate and charged for use by the minute, so it was desirable to devise a method of running as many mPADs through the device as possible per session.

To account for this, the mPADs coverslips were arranged in groups of 12 on clean blank silanized 4-inch silicon wafers. For each wafer, PDMS was prepared at a 10:1 base-to-cure ratio and degassed for 30 minutes and then spun onto a wafer loaded onto a model G3P spin coater (Specialty Coating Systems, Inc., Indianapolis, IN, USA). The PDMS was spun at 500 rpm for 60 seconds and then baked at 90 °C for 60 minutes. Once removed from the oven, the glass coverslips were carefully dropped onto the PDMS

surface, feature side up. If the PDMS was clean of any dust or debris, the coverslip would quickly adhere to the flat PDMS surface. This temporary bond between the glass and PDMS was strengthened by heating wafer again with the mPADs for a further 60 minutes in at 90 °C (Bhattacharya et al., 2005). Note that this additional heating step would affect the cumulative baking time for PDMS and could lead to additional cross-linking. Therefore, all mPADs used were subjected to critical point drying, even if the post arrays were already flawless.

The 4-inch wafers with mPADs were then placed in a 1000 mL beaker filled with enough technical grade 99% ethanol (Merck KGaA, Darmstadt, Germany) to cover the mPADs surface by about 1 cm. The beaker was sonicated in a Branson model 2510 ultrasonic cleaner (Marshall Scientific, Hampton, NH, USA) for 90 to 120 seconds or until most mPADs post array regions appeared to refract light. Once ready, the wafers were quickly transferred to a wafer-carrying puck which was also filled with technical grade ethanol, being careful to keep the mPADs features continuously fully wetted. The pucks were not watertight and needed to be wrapped in parafilm to prevent loss of ethanol during transfer between buildings.

The wafers were carefully transferred from the Alford lab space in Nils Hasselmo Hall to the Keller Hall MNC clean room which housed the critical point drier. Three to five wafers containing mPADs were loaded into the 4-inch wafer caddy already sitting in another technical grade ethanol bath with spacer rings between each wafer. The wafers were rinsed in another two ethanol baths before being loaded into the critical point drier, which itself was prepared with ethanol in its chamber. After the machine ran and

completed its operational cycle, the now-dry wafers were removed from the chamber and transferred back to the Alford lab. The mPADs were carefully peeled off the wafer and stored in clean 6-well dishes. Finally, the mPADs were inspected for quality after the critical point drying. Devices with large regions of flawless micropost arrays were saved for experiments and those without were discarded.

2.3 Creating mPADs "sandwich spacers"

In order to create a predictable, controllable space between the confronting functionalized mPADs surfaces a robust method was needed to manufacture and apply a barrier to act as the middle layer in the mPADs "sandwich." The objective was to create barriers with discretely stepped thickness in a range slightly smaller than the circumference of a fully suspended HUAVSMC (approximately 10-20 μm typically observed during subculture). The barrier needed to fit along the thick wall of the mPADs design (Figure 1) without blocking the micropost features. No existing pre-fabricated materials available in the lab were simultaneously within the desired thickness range and easily manipulated for this application. Multiple attempts were made before a reliable solution was found.

2.3.1 Tape-protected PDMS Spin onto Coverslip

The first attempt was to place thin strips of transparent office tape on a silanized 25 mm circle coverslip, then coat the coverslip with different recipes of PDMS, and then

remove the tape prior to baking the remaining coverslip at 90 °C for 60 minutes, as shown in Figure 7 below.

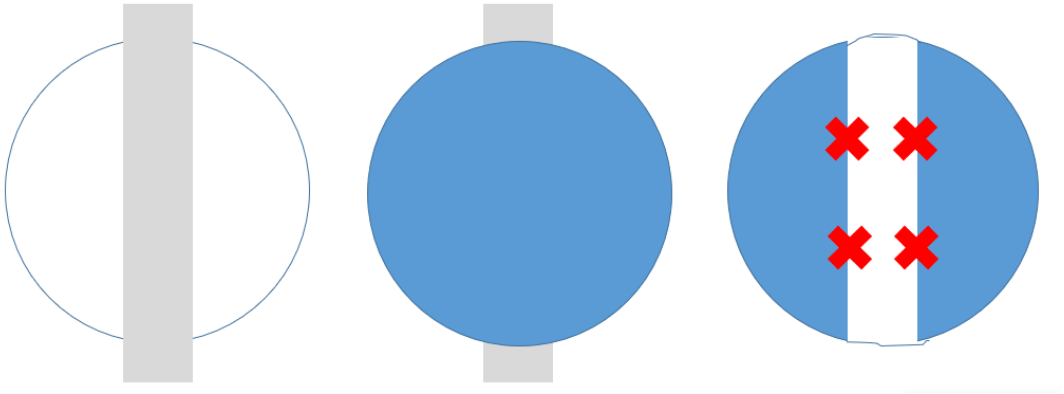

Figure 7: Left: Tape applied to coverslip. Middle: Coverslip and tape spun with PDMS (blue). Right: tape peeled off

Four test conditions were attempted by using two spin coating recipes, and two different PDMS formulations, per Table 5 below.

Table 5: Spin coater recipes for tape removal protocol

Spin Coater Recipe	PDMS Formulation
3000 rpm for 60 seconds	100% 10:1 base:cure 184 Sylgard PDMS
5000 rpm for 60 seconds	67% 10:1 base:cure 184 Sylgard PDMS 33% 190 proof Ethanol

At least two coverslips were prepared in each of the four possible conditions. To measure the height and cross-sectional profile of the remaining cured PDMS on each sample, the samples were taken to the Keller Hall MNC Clean Room for observation in the P-16 Surface Profiler (KLA Tencor, Milpitas, CA, USA). An approximately 1 mm measurement was taken starting at the PDMS surface and measuring the surface height perpendicular to the line created by the tape removal, extending approximately 0.1-0.2 mm into the glass region. Note: due to the possibility of loose fragments of PDMS or other debris getting stuck on the Surface Profiler stylus, the measurements for each device could not be made at the exact same position on each coverslip. Instead, measurements were made approximately 1-2 mm from the edge of the coverslip, but in a straight-line region free of debris which might damage the equipment.

It was clear that the relatively thick tape layer created variance in the final PDMS thickness with large peaks in PDMS at the tape edge line (Figure 8: Surface profilometer measurement of the side wall for the tape removal protocol). While less-pronounced when using PDMS diluted with ethanol, this process yielded an non-uniform sheet of PDMS. In order to reliably separate the confronting functionalized mPADs surfaces, the PDMS barrier would need to be predictable and level.

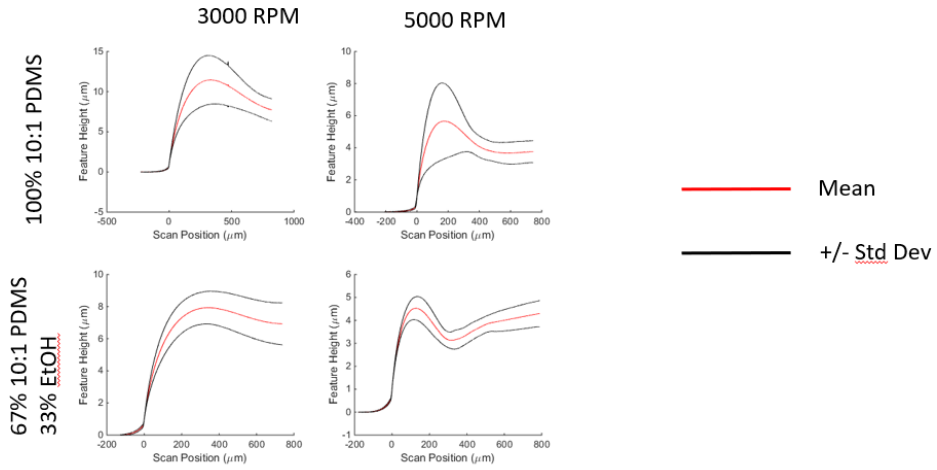

Figure 8: Surface profilometer measurement of the side wall for the tape removal protocol

It was determined that this method would not be suitable to create mPADs sandwich barriers without modification to account for the non-uniformity created by the tape.

2.3.2 PhotoPDMS

The next attempt to create mPADs barriers was via the use of *photoPDMS*, a modified light-sensitive modified form of PDMS which could be patterned with rudimentary photolithography. PDMS was first modified for photoreactivity by Lötters *et al* in 1997 by preparing a PDMS mixture with 1% (by weight) DMAP (2, 2-dimethoxy 2-phenylacetophenone).(J C Lötters, 1997) This first technique took several hours and

required special machinery. Later, Tsougeni *et al* demonstrated the use of three other free radical photoinitaitor co-polymers along with the PDMS base polymer to allow the resultant polymer to be selectively patterned with exposure to UV in a mask aligner.(Tsougeni et al., 2007) These co-polymers all featured vinyl-methyl siloxane groups which could be sensitized to 300-400 nm UV light.

A simpler and less expensive method was published by Jothimuthu *et al* in 2008 (Jothimuthu et al., 2009). Benzophenone has long been used to produce free-radicals from to crosslink under UV light (Müller et al., 1991), Müller et al., 1992). Using 3% benzophenone (by weight) in the typical 10:1 base to curing agent Sylgard 184 PDMS mixture, Jothimuthu *et al* successfully produced 100 µm-scale features using only transparency masks and a portable light source, outside of the clean room and insensitive to ambient light. Hypothetically, this preparation of photoPDMS could be utilized to create uniform mPADs sandwich barriers. The barriers themselves only needed to be accurate to 100 µm (~2 mm wide), so long as their thickness was consistent across the entire surface.

As shown in Figure 9, photoPDMS could be spun onto a pre-fabricated mPADs (a-b) device and placed under a simple photomask to selectively expose the functionalized post regions to ultraviolet light (c). The exposed photoPDMS could then be dissolved in a developing reagent leaving only a perimeter wall of PDMS (d-e) onto which a second mPADs device could be placed (f).

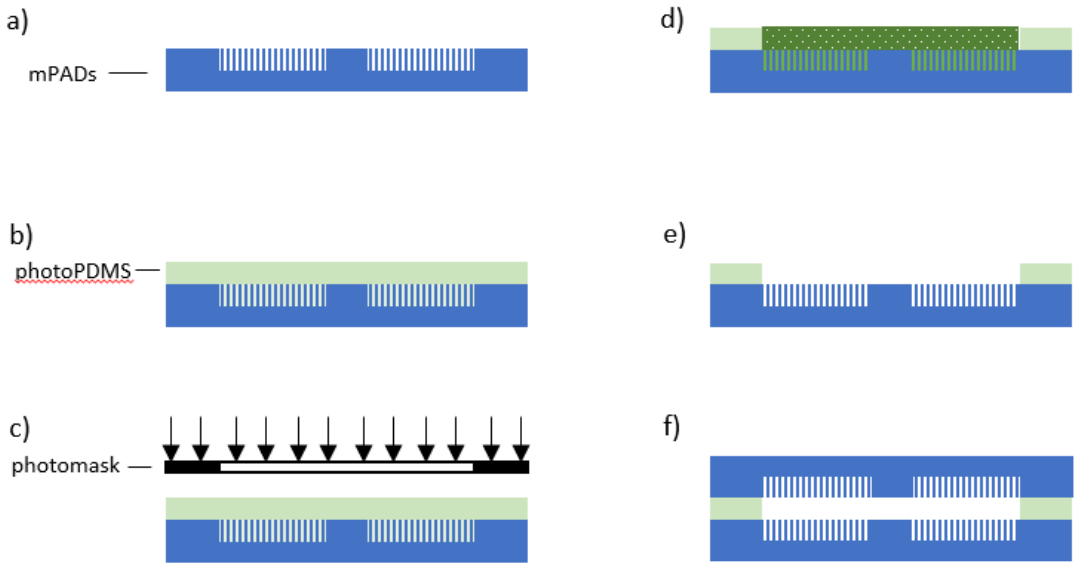

Figure 9: photoPDMS protocol

This method would require complete dissolution of exposed photoPDMS in the developing agent followed by thorough rinsing of the original mPADs substrate to avoid additional polymer remaining between the microposts and affecting the functional rigidity of the array.

The following protocol was used to test the feasibility of photoPDMS as mPADs as "sandwich spacers" based on the Jothimuthu *et al* method described above. Coverslips (25CIR.-1, Fisherbrand) were prepared by spinning degassed 10:1 Sylgaard 184 PDMS base:cure at 1800 RPM for 60 seconds and baking for 60 minutes at 90 °C to fully cure. This batch of coverslips would stand in as the mPADs substrate upon which PDMS would be spun.

To prepare photoPDMS, 0.1 g benzophenone (Sigma Aldrich, Darmstadt, Germany) was dissolved in approximately 0.15 g xylene (Sigma Aldrich, Darmstadt, Germany) and then mixed into 0.3 g Sylgard 184 PDMS curing agent. This mixture was then mixed with 3.0 g Sylgard 184 PDMS base polymer in a Thinky AR-100 planetary centrifugal mixer (Thinky USA, Inc., Laguna Hills, CA, USA). The resultant photoPDMS mixture contained ~2.8% benzophenone. From this point on, the photoPDMS was protected from ambient light by aluminum foil to avoid unnecessary exposure to ultraviolet light. The mixture was degassed and spun onto the prepared coverslips at 2000 RPM for 60 seconds. The photoPDMS would be a second layer of substrate on top of the unmodified PDMS base layer.

As a feasibility experiment, a photomask was fabricated by printing a simple pattern onto a sheet of photo transparency paper consisting of alternating 1.5 mm thick opaque and transparent regions (Figure 10).

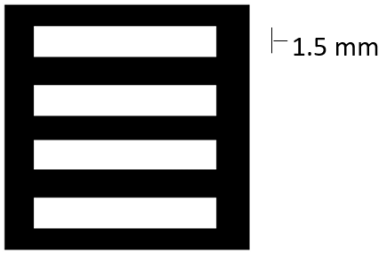

Figure 10: photoPDMS feasibility test photomask

The transparency paper photomask was glued onto a glass microscope slide and positioned above the photoPDMS spun coverslip using additional coverslips on the

lateral edges of the microscope slide to prop the photomask up such that the printed photomask surface was had minimal clearance above the uncured photoPDMS without making contact. Given that PDMS has an approximate thickness of 0.04 mm when spun at 1800 to 2000 RPM, there were two layers of PDMS on the coverslip, and the coverslip itself is cited as 0.13-0.17 mm, the total assembly would be approximately 0.3 mm tall (Koschwanez et al., 2009).

The wall features needed for the mPADs sandwich barrier were large enough such that the theoretical near field Fresnel diffraction limit should not have posed a significant trouble. Since the barrier walls did not need to have precisely defined edges, a feature resolution of ~0.1 mm should have sufficed. The maximum exposure gap between the mask and the substrate, g was approximated as the feature size, W squared and divided by the wavelength, λ,

$$g_{max} = \frac{W^2}{\lambda} \quad . \tag{4}$$

Conservatively requiring a feature resolution of 0.1 mm and an exposure wavelength of 400 nm, the estimated allowable gap was 2.5 cm. In practice such a gap would, at best, test the limits of the above approximation, but did re-assure that a mask-to-substrate gap of less than a millimeter should have sufficed. Using different cover slips readily available in the lab should have provided minimal but existent photomask clearance above the photoPDMS. Per the specifications given by Fisherbrand, the model 12-540A square coverslips should be 0.17-0.25 mm and the model 12-545-102 circle coverslips

should be 0.13-0.17mm. Using one of each would provide a total height of 0.30 – 0.42 mm leaving a gap, *g* of 0.00-0.12 mm.

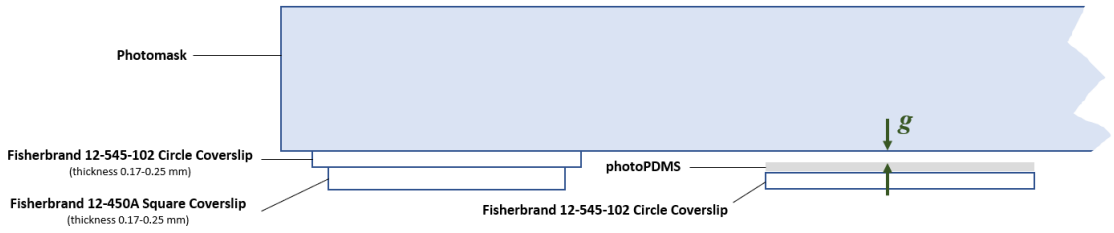

Figure 11: photoPDMS feasibility experiment setup

Using this setup, the photoPDMS, the and the photomask were loaded into a Jelight Model 42 UV Ozone cleaner (Irivine, CA) and exposed for 5 minutes, as close to the lamp as possible. The coverslip was then immediately baked for 60 seconds on a hot plate set at 120 °C to soft bake. The coverslip was then rinsed with ~0.5 mL Toluene and dipped in methyl-isoutyl ketone (MIBK) for 20-25 seconds to develop, followed by hard baking on the same hot plate until fully cured.

After attempting this experiment several times, the resulting photoPDMS coverslips were examined using a KLA Tencor Surface Profiler (Capovani Brothers, Inc, Scotia, NY). The surface profile results showed that photoPDMS discouraged further investigation or optimization of the process. As seen in the representative ~10mm surface profile measurement below (run perpendicular to the features, as in Figure 12 below), this rudimentary setup failed to create resolved figures.

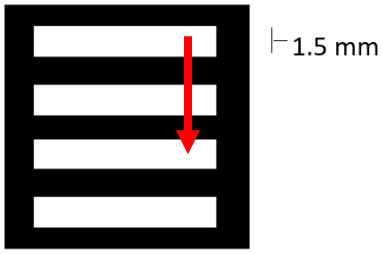

Figure 12: Direction of surface profilometer measurement

Although there were distinct peaks and valleys, roughly aligning with the pattern printed on the photomask, there were problems with the resulting surface which were ultimately prohibitive for use of this apparatus to fabricate mPADs sandwich barriers. Regardless the physical height of the yielded "features," the resulting photoPDMS substrate had very poor feature resolution. Two possible issues dooming this cheap setup were the inability to reduce the gap between the wet, uncured photoPDMS and the mask, and the inability to solely focus the UVO cleaner's light onto the mask. To address the gap, additional experiments were attempted by gently placing the mask directly onto the photoPDMS, to be peeled off later, but the direct contact of the transparency plastic to the PDMS sample created an uneven an unpredictable surface flaws.

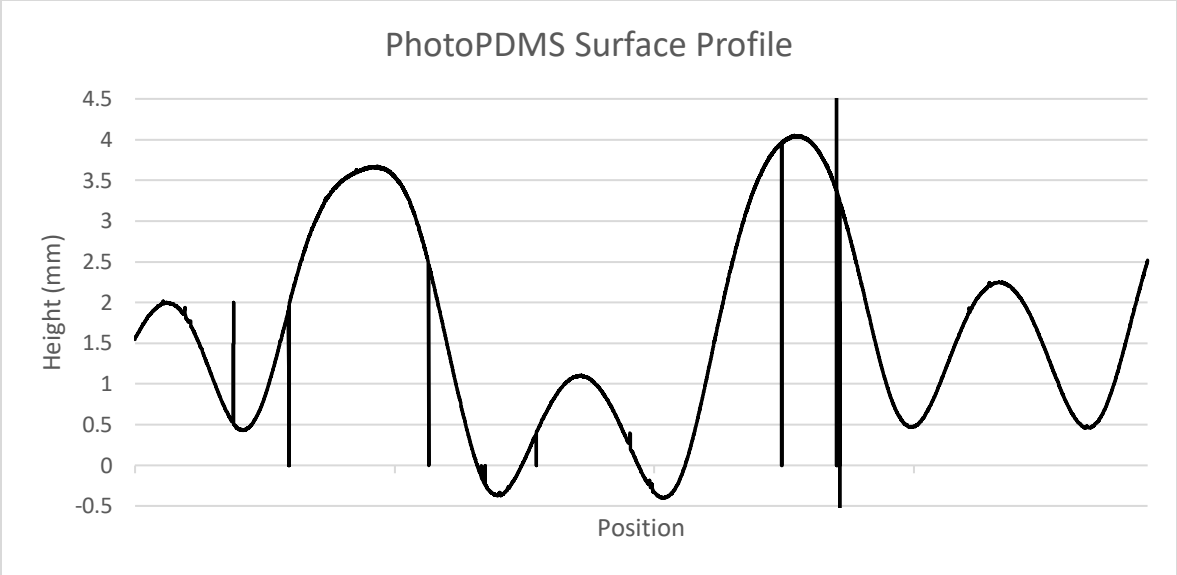

Figure 13: Sample surface profilometer measurement for photoPDMS feasibility experiment

2.3.3 Bonded Flat Stamp Peel-off

What ultimately succeeded in creating predictable, reproduceable mPADs sandwich spacers was a the bonding and peeling-off of ~1 cm thick, 12 × 25 mm PDMS flat stamps to thin films of PDMS spun onto silanized coverslips. This method allowed for consistency in PDMS wall thickness by standardizing the spinner recipe, creating uniform thin films, and cleanly removing a 12 mm-wide strip from the coverslip substrate, leaving a relatively clean edge and well-defined sidewall barrier.

2.3.3.1 PDMS thin film fabrication

To begin, 25 mm circular 0.1mm thick coverslips (Fisherbrand model 12-545-102) were sonicated for 30 minutes in 70% ethanol for cleaning and then allowed to dry overnight in a closed fume hood. The clean coverslips were then placed in a plasma cleaner (Harrick model PDC-32G) for 60 seconds each on the "high" setting.

The cleaned and freshly-plasma-treated coverslips were then silanized by being placed in a vacuum desiccator (Bel-Art products model 999320237) along with 4 drops of trichloro (1H, 1H, 2H, 2H-perfluorooctyl) silane (Sigma Aldrich) for 4 hours. The purpose of this silanization is to allow the clean delamination of future PDMS to be spun onto the coverslip.

A small volume (~20-25 g) of Sylgard 184 PDMS was prepared (10:1 base:cure) was measured out, mixed (Thinky model AR-100), and placed in a vacuum desiccator for 20 minutes. The silanized coverslips were loaded one-at-a-time onto a spin coater (Specialty Coating Systems model G3P), and a ~1cm diameter pool of PDMS was pipetted on the center of the coverslip. For the purposes of characterizing the resultant thin films, the following recipe was used.

Table 6: Flat stamp peel-off protocol spin coat recipe at various speeds

Step	**Target Rotational Speed (RPM)**	**Hold Time at Target (s)**	**Ramp Time (s)**
0	0	0	0
1	500	5	5

2	1000	5	5
3	*x*	180	10
4	1000	5	5
5	500	5	5
6	0	0	5

x = 2000, 4000, or 6000

The total spin time (time held at target RPM plus time elapsed during ramp) for each recipe was 235 seconds, but during step 3 the target rotational speed was set to either 2000, 4000, or 6000 RPM.

A total of nine samples were coverslips were prepared for spinning. Assuming one or two minutes of time could be spent unloading the previous coverslip and loading the next one, nearly an hour would elapse between the degassing of the PDMS and the spinning of the final coverslip, samples were prepared in the following order to mitigate any confounding effects of PDMS curing at room temperature.

Table 7: Sample Rotational Speed Order

Sample	**Rotational Speed (RPM)**
1	2000
2	4000
3	6000
4	2000

5	4000
6	6000
7	2000
8	4000
9	6000

The PDMS-spun coverslips were then returned to the vacuum desiccator overnight for curing and residual degassing. The following day, samples were removed from the desiccator and baked for 30 minutes at 90 °C for a final hard cure.

2.3.3.2 PDMS flat stamp fabrication

A brand new 4-inch silicon wafer (WaferPro, Santa Clara, CA) was prepared by performing successive rinses with acetone and isopropyl alcohol, followed by drying with nitrogen air. The wafer was silanized for four hours in the vacuum desiccator with four drops of trichloro (1H, 1H, 2H, 2H-perfluorooctyl) silane (Sigma Aldrich, Darmstadt, Germany).

To create PDMS flat stamps, a larger volume (~100g) of 184 Sylgard PDMS (10:1 base:cure) was mixed (Thinky model AR-100, Laguna Hills, CA) and degassed (Bel-Art products model 999320237) for 60 minutes. The PDMS was then poured over the prepared wafer inside a plastic petri dish in a ~1 cm thick layer and baked overnight at 90 °C. The following day the PDMS and wafer were carefully removed from the petri

dish using a box cutter. The PDMS was peeled away from the wafer, keeping the wafer flat on the bench top to prevent cracking. Keeping the flat wafer-side surface of the PDMS brick facing upward to prevent scratching, the PDMS was then dissected into 12 × 25 mm stamps using a single edge razor blade. A small notch was cut into the non-functional side of each stamp to indicate proper orientation. Just prior to use, the flat stamps were then sonicated (Branson model 2510, Marshall Scientific, Hampton, NH) in 70% ethanol for 30 minutes and then nitrogen dried.

2.3.3.3 Stamp bonding and peel-off

To bond the stamps to the PDMS-spun coverslips, both were placed in the plasma cleaner at the same time while the machine was run on the "high" setting for 60 seconds. Immediately following the completion of the plasma treatment, the functional surface of the stamp was lined up across the diameter of the coverslip. The stamps were gently depressed to ensure no air bubbles were caught between the stamp and the PDMS film.

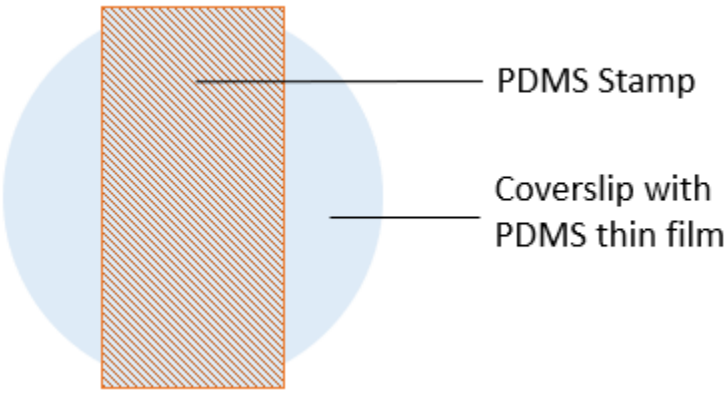

Figure 14: PDMS stamp placement on PDMS-spun coverslip

To strengthen the bond, the coverslip/stamp constructs were baked for 30 minutes at 90 °C. After baking, a razor was used to cut along the length of the stamp. Finally, the stamps were peeled off by holding the coverslip flush against the lab bench and carefully lifting off the stamp, starting at one end near the edge of the coverslip. What remained was two half-moon shaped regions of thin film which, by nature of the silanized glass substrate, could be transferred to another PDMS device later on.

2.3.3.4 Characterization

With all the PDMS films now created, a surface profiler (Tencor model P-16) was used to measure the thickness the resulting PDMS films at various points on its surface. Measurements of each sample were made at up to six locations, fewer if debris or delaminating PDMS put the profiler stylus at risk of damage at the measurement location. The outermost edge was not measured as a ~1 mm edge beading of PDMS was visible on each sample, which could easily be cut away prior to any thin film usage in a final mPADs sandwich. Note that the measurement locations were not precise from sample to sample.

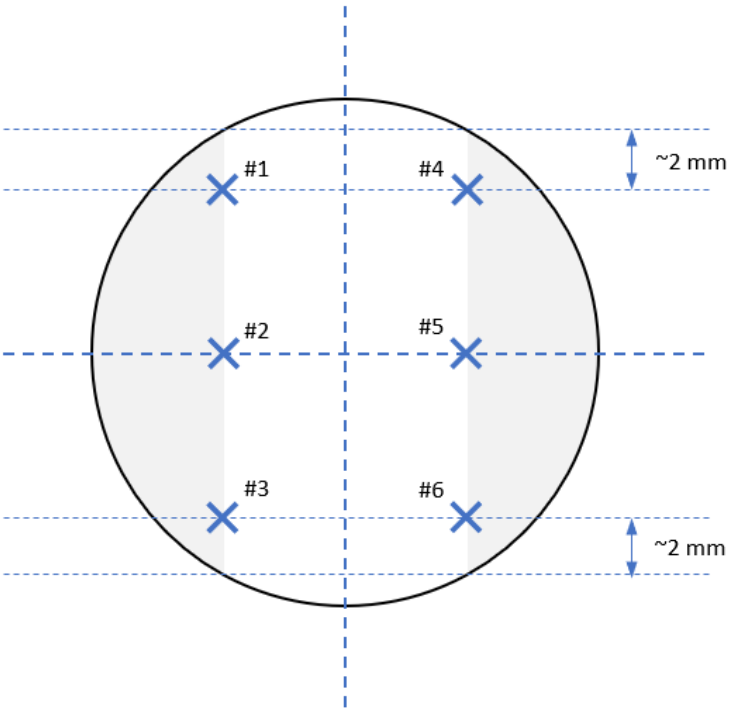

Figure 15: Measurement locations on surface profilometer

Immediately, the large variances near the step between the PDMS wall and the coverslip were noticeably absent. Across all speeds, the method of spinning PDMS across a flat surface, letting it cure, and *then* removing the unwanted strip along the center axis hurdled this previous obstacle.

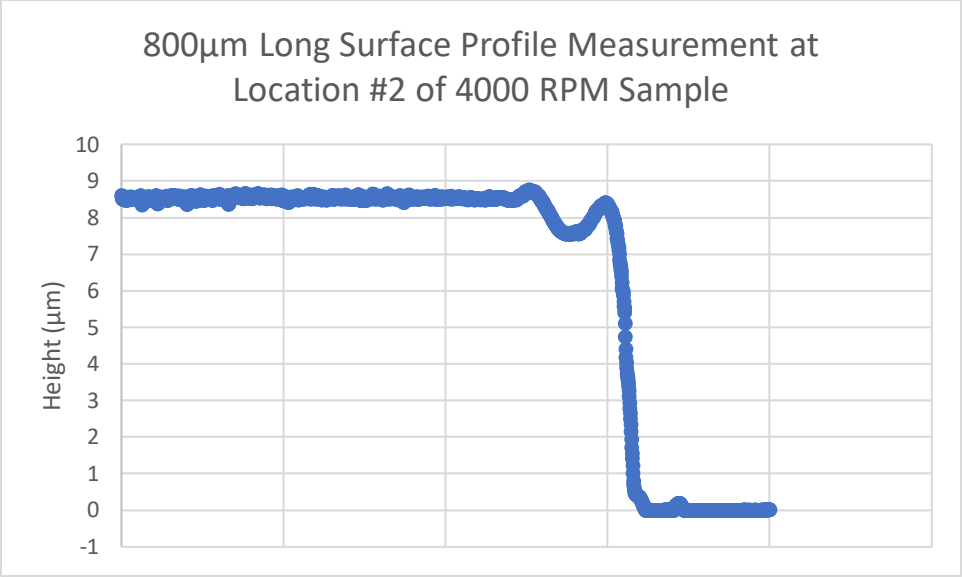

Figure 16: Sample surface profilometer measurement for bonded flat stamp peel off protocol

In Table 8 below, wall height at the center (H_{center}) was measured by compiling the results from measurements at locations 2 and 5, while the wall height at the edge (H_{edge}) was measured by compiling the results from measurements at locations 1, 3, 4, and 6.

Table 8: Surface profilometer measurements for bonded flat stamp peel off protocol

Spin Speed, ω (RPM)	**Average Wall Height at Center, H_{center} (µm) ± s.d.**	**No. of meas.**	**Average Wall Height at Edge, H_{edge} (µm) ± s.d.**	**No. of meas.**	**Average Difference In Height from Edge to Center, ΔH (µm)**
2000	16.70 ± 0.47	5	30.59 ± 1.45	12	13.88 (83.1%)

4000	8.58 ± 0.09	5	9.87 ± 0.78	11	1.29 (15.1%)
6000	5.71 ± 0.16	6	5.76 ± 1.78	9	0.05 (0.9%)

The results were fit to the following power function where *C* is the polymer solution concentration, η is the intrinsic viscosity of the polymer, and α, β, and γ are calibration constants.(Zhang et al., 2004)

$$H = KC^{\beta}[\eta]^{\gamma}\omega^{\alpha} \quad (5)$$

Since only PDMS at one prepared concentration (10:1 base:cure) is being used, no variance in polymer viscosity was expected, and it was acceptable to simplify the equation using two constants, k_1 and k_2.

$$H = k_1\omega^{k_2} \quad (6)$$

Using the mean center heights measured, k_1 and k_2 were calculated to be 2.77×10^4 and -9.75×10^4, respectively.

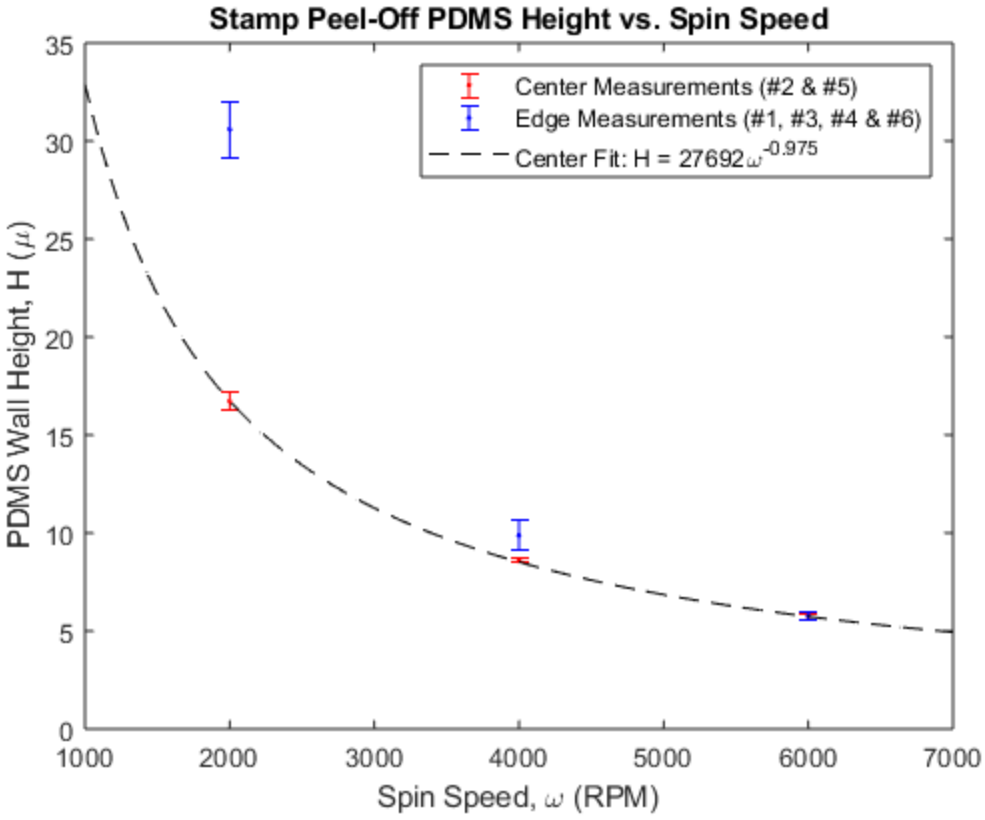

Figure 17: Exponential fit for PDMS wall height versus spin speed

Creating PDMS thin films by spinning at 2000 RPM on the 25 mm coverslip created far too drastic of edge effects to be relied upon for this experiment. However, spinning at 4000 and 6000 RPM produced discrete wall heights with significantly less edge beading. The roughly 3μm (50%) difference in height between 4000 and 6000 RPM was large enough to continue with fabricating mPADs sandwiches under this protocol.

Aside: This protocol would later be repeated for use in future experiments, but spinning at 5000 RPM in order to test an intermediate spacing between 4000 and 6000

RPM. The theoretical thickness of this barrier based on equation (6) is approximately 6.8 μm.

2.3.3.5 Functionalization and Final Assembly

To ensure that the PDMS walls could be adhered to single-sided mPADs fabricated on 18 × 18 mm square coverslips, several new, silanized coverslips were spun with PDMS at 4000 RPM and 6000 RPM per the protocol described above, followed by center strip removal using the flat stamps. The mPADs and thin film coverslips were then placed into the plasma cleaner and cycled on the "high" setting for about 45 seconds. Upon removal from the plasma cleaner chamber, the coverslip apparatuses were immediately pressed together PDMS-to-PDMS and baked for 15 minutes at 90 °C.

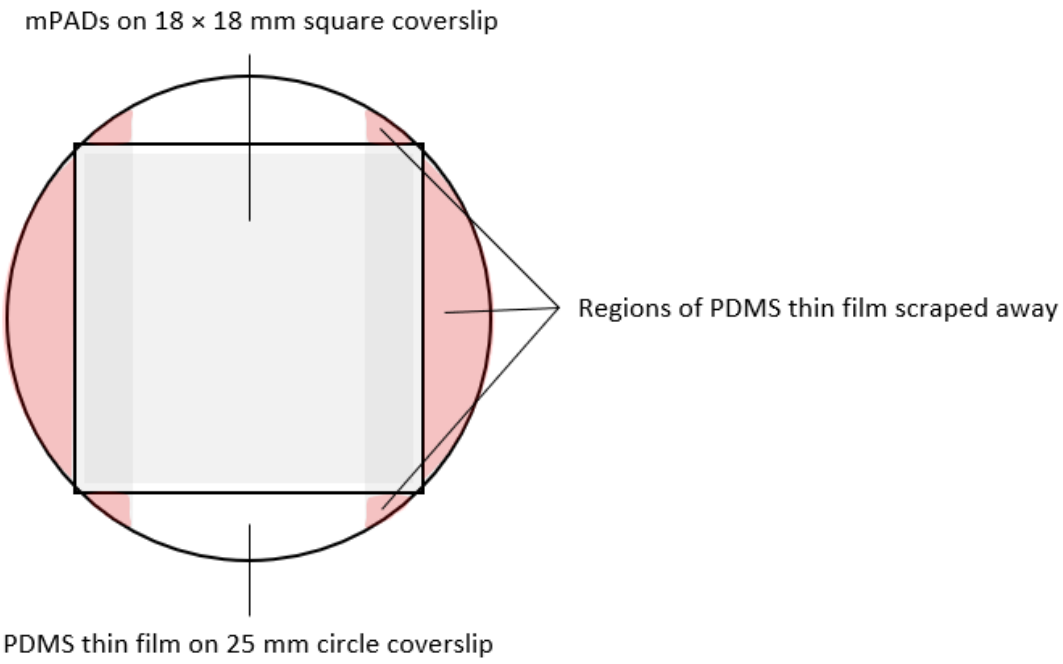

Figure 18: Schematic of mPADs placement on thin film barrier spun on coverslip

Upon removal from the oven, the thinner 25mm thin film coverslip would be braced flat on the lab counter using one pair of tweezers. the thicker mPADs square coverslip would be carefully lifted of using another pair of tweezers.

2.4 Attempted Use with Live Cell Migration

2.4.1 Purpose and Hypothesis

The intended use of the pseudo-3D mPADs device was to study the effect of substrate stiffness and spacing on cell migration in a three-dimensional (i.e., not spread)

state. The intent was to place cells in mPADs devices with various micropost stiffness and various top-to-bottom mPADs spacing.

Hypothesis: In-plane cell migration speed will not occur with insufficient space between the two mPADs. The migration speed will vary as some function of space as the space between the mPADs increases to an optimal point where the cell can utilize both the superior and inferior substrates for migration. Once the spacing between the mPADs eclipses a maximum distance, the cells will no longer be able to interact with the superior substrate and the cell will return to its normal spread state migration on the inferior mPADs. The hypothesized cell migration speed on a given substrate/micropost stiffness is described by the following equation where v is in-plane cell migration speed, s is the mPADs-to-mPADs spacing, S_{min} and S_{max} are the minimum and maximum space required for cells to interact with both top and bottom devices, and v_{spread} is the basal migration rate of a cell spread on a flat surface. The function $f(s)$ is an arbitrary function with of migration speed with respect to spacing.

$$v = \begin{cases} 0 & ,if\ s < S_{min} \\ f(s) & ,if\ S_{min} \leq S < S_{max} \\ v_{spread} & ,if\ s \geq S_{max} \end{cases} \tag{7}$$

2.4.2 Experimental Procedure

The following sections detail the experimental procedure used to image six separate pseudo-3D mPADs sandwich devices seeded with Human Umbilical Artery Smooth Muscle Cells (HUASMC). HUASMCs are vascular smooth muscle cells harvested from normal arteries within the human umbilicus.

2.4.2.1 Functionalizing mPADs

2.4.2.1.1 Flat Stamp Preparation

Flat stamps were prepared using a similar method as described in section 2.2.3.ii above, mixing 10:1 base:cure Sylgard 184 PDMS. PDMS was poured onto a silanized blank 4-inch wafer, baked fully at 90 °C overnight, and then dissected into 11 × 17 mm flat stamps. A small notch was cut into the back side of the stamps for reference. The stamps were then cleaned by sonicating in 70% ethanol and dried with nitrogen until needed.

A combination of fibronectin (FN) (Cytoskeleton, Denver, CO) and rhodamine-labeled fibronectin (RhoFN) (Cytoskeleton, Inc., Denver, CO , USA) was used to functionalize the cell-facing micropost surfaces and to make the posts visible with fluorescent imaging. Two (2) prepared suspensions of 50 µL of 1.0 mg / mL FN were added to 950 µL of phosphate buffered saline (PBS) and placed on an ice bath for 30 minutes. At the same time, 20 µL of sterile water filtered water was slowly pipeted into each of two (2) off-the-shelf vials of 20 µg RhoFN, letting the solutions re-suspend for 2-3 minutes. Each RhoFN suspension was then diluted in 180 µL PBS and placed on ice with the FN suspension, shielded from ambient light. After the 30-minute re-suspension on ice to the final concentrations, the FN and RhoFN solutions were combined for two (2) vials with final volume of 1200 µL each.

Table 9: Mixed fibronectin preparation:

Solution	Mass	Initial Volume	Initial Concentration	Combined Concentration
FN	50 µg	1000 µL	50 µg/mL	41.7 µg/mL
RhoFN	20 µg	200 µL	100 µg/mL	16.7 ug/mL

In an unlit fume hood, 200 µL the FN + RhoFN solution was pipeted onto each of twelve (12) clean 11 × 17 mm flat stamps, wetting the entire surface area of each stamp using the pipet tip. The fibronectin solution was left to incubate on the stamp in a dark hood for 60 minutes. After incubation, the stamps were dried with nitrogen and protected from ambient light in the fume hood until needed.

2.4.2.1.2 Functionalizing mPADs Posts

Twelve (12) pre-prepared single-sided mPADs were prepared – six (6) prepared according to the protocol described in section 2.2.2 and another six (6) prepared the same way, but with added according to section 2.3.3. (Note: only 3.5-µm and 3.0-µm-post-devices were used as these were the most abundantly available and being the most likely to survive the master mold peel off and CPD drying procedure described earlier.) The non-wall mPADs were placed into one six-well dish and the side-wall-added mPADs were added to another.

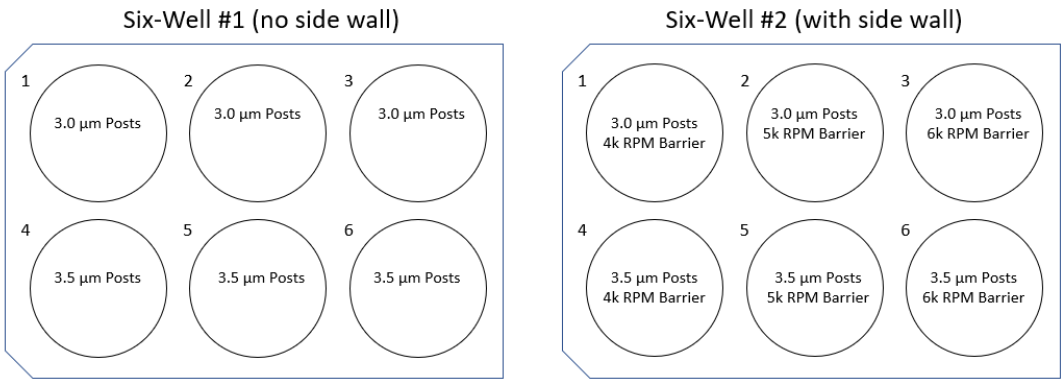

Figure 19: Placement of devices within six well dishes

Both six-wells were placed in a Model 42 Series UVO-Cleaner (Jelight Company, Inc., Irvine, CA) for 8 minutes in order to increase the concentration of hydrophilic groups on the micropost surfaces in preparation for stamping with fibronectin.(Özçam et al., 2014) Once UVO treatment was complete the six-well dishes were moved to the unilluminated fume hood with the fibronectin-incubated stamps. One-at-a-time, the stamps were carefully dropped onto the microposts, aligning the center of the stamp over the center of the mPADs and ensuring that the stamp fell lengthwise parallel to the barrier side wall, if present. Each of the twelve (12) stamps was then gently tapped to ensure complete contact with the micropost tops and then carefully peeled off.

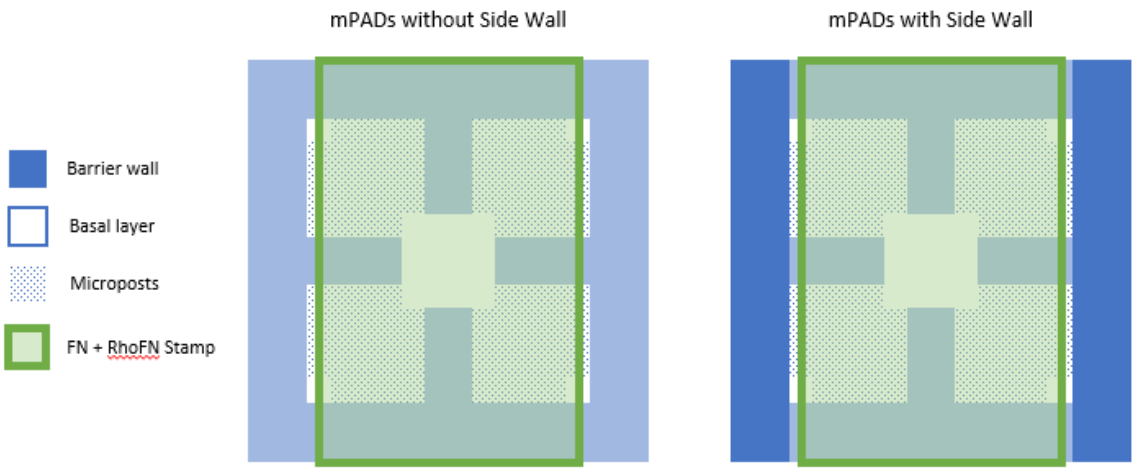

Figure 20: Schematic of FN-coated flat stamp onto mPADs

Next, a treatment of 1% Pluronic® F-127 (Sigma Aldrich, Darmstadt, Germany) was needed to inhibit cell adhesion elsewhere in the deice (i.e., anyplace other than the stamped post tops). The polyethylene oxide (PEO) chains in Pluronic compete with other surface proteins (in this case fibronectin) and, in effect, only allow cell adhesion on surfaces where both the Pluronic and the FN + RhoFN molecules are present.(Higuchi et al., 2003)·(Maazouz et al., 2017)

One primary concern with the fine micropost structure of the mPADs devices fabricated elsewhere has been the risk of micropost collapse upon immersion in a solution with high surface tension.(Sniadecki and Chen, 2007) Instead of immediately immersing the devices into the water-based Pluronic solution and then rinsing with PBS, the following rinse protocol was set up to wet the mPADs with ethanol, which has a lower surface tension than water (72.9 $mN \cdot m^{-1}$ for water-air versus 22.5 $mN \cdot m^{-1}$ for

ethanol-air at 20 °C). At each step each well was filled with approximately 2 mL of the prescribed solution, and each well was aspirated immediately prior to filling with the next solution to minimize the risk of the micropost arrays completely drying again. After filling the wells with Pluronic, the solution was left to sit for 30 minutes without aspirating to allow the PEO chains to adhere.

Table 10: mPADs surface wetting procedure

Wash Step	Solution	Duration
1	Pure ethanol	1 minute
2	70% ethanol in water	1 minute
3	70% ethanol in water	1 minute
4	1% Pluronic in water	30 minutes
5	1× PBS	1 minute
6	1× PBS	1 minute

The mPADs devices were left in PBS until ready for cell seeding. The mPADs with side walls were designated as the “bottom” layer and the mPADs without side walls were the “top.”

2.4.2.1.3 Cell Culture Preparation

For this experiment HUASMCs were dyed with CellTracker ™ Green CMFDA Dye (ThermoFisher Scientific, Waltham, MA, USA) for fluorescent visualization. The

DMFDA dye powder came in pre-allotted 50 µg aliquots and was stored at -15 °C. One unit of the powder was allowed to return to room temperature 60 minutes prior to use, and then dissolved in 1.08 µL dimethyl sulfoxide (DMSO) to achieve a working concentration of 10 mM.

Meanwhile, HUAMCs were prepared for seeding. All cells used were cultured according to the manufacturer recommendations and between subculture counts 4 and 7. To resuspend the cells, the existing media was aspirated from a T75 flask with HUACMs at 80% confluence and then rinsed with PBS. The PBS was aspirated and 1.5 mL Trypsin (0.05 %wt/vol) in ethylenediaminetetraacetic acid (2 mM) was added and the flask was incubated for 3-5 minutes while the trypsin resuspended the cells. The trypsin was then neutralized with 8.5 mL warm media. The media was transferred to a 15 mL centrifuge tube and placed in a centrifuge at 250 relative centrifugal force (rcf) for 5 minutes. Out of the centrifuge, the remnant media + trypsin solution was as aspirated, leaving a pellet of HUAVCs at the bottom of the tube. The pellet was resuspended in 5 mL warm media, gently pipetting the solution up and down 10-15 times. The cellular concentration was approximated using a hemocytometer. Finally, the CMFDA dye in DMSO was added to the suspended cells, and the cells were left to incubate in a 37 °C bath, shielded from light, for approximately 30 minutes. From this point forward, the cells were shielded as much as possible from ambient light.

2.4.2.1.4 Cell Seeding and Observation

Given the cellular concentration determined earlier, enough media corresponding to 30,000 cells was placed in each of the six bottom mPADs wells (with side walls), or approximately 3,000 cells/cm^2. Each well was then topped off with media to reach a final volume of 2 mL per well. Both the bottom mPADs six well and the top mPADs six well were placed in an incubator for 60 minutes to allow the cells to begin attaching and spreading to the bottom devices' micropost tops.

Both six wells were then removed from the incubator and placed in an unlit fume hood. Each top mPADs device was then removed from its well and placed upside down on top of the corresponding bottom mPADs device (e.g., top well #1 → bottom well #1, etc.). The coverslips were aligned, and a small dab of silicone gel was placed on the side of the mPADs sandwich to prevent movement.

Additionally, a second control preparation of six (6) "traditional" non-sandwich mPADs were assembled and seeded with cells in a similar manner. These "one-sided" mPADs were used to demonstrate that the devices themselves were functioning properly and allowing cell adherence. (Note that these one-sided devices were prepared on a separate date as the confocal microscope could only accommodate one 6-well dish at a time).

One hour prior to observation, the microscope was turned on with the stage chamber pre-heated to 36 °C. Once all mPADs sandwiches (or one-sided devices) were prepared and stabilized with silicone gel, the "top" six well, the tray was moved to the

Olympus IX81 confocal microscope (Olympus Corporation, Tokyo, Japan) for observation.

Each well was scanned to find an aligned region with flawless microposts on both the top and bottom mPADs. This location was then saved in the image processing software MetaMorph Advanced (Version 7.10.2.240, Molecular Devices, LLC, San Jose, CA), as measurement site. No auto-focus features were used since this could strain the computer resources and result in data loss or premature termination of the measurement. Instead, each programmed image capture was accompanied by approximately ten additional photos at field depths slightly above and below the initial "in-focus" zoom to account for any shifting during the experiment. The imaging software was programmed to take a stack of images of each "good" region found in the six-wells every five minutes for 8 hours. Each image was taken using the bright field, the FITC filter to image the CellTracker Green embedded within the HUASMCs, and the TRITC filter to image the Rho-labeled Fibronectin stamped on top of the microposts.

2.4.2.1.5 Image Processing

Each capture was saved as a stacked Tag Image File Format (TIFF) file containing all stepped zoom depths recorded. As this resulted in thousands of files, a Matlab (The MathWorks, Inc., Natick MA) .m file (Appendix A) was written to identify the most in-focus image in each TIFF stack. Brenner's equation for image focus quality (Brenner et al., 1976) was applied to each image to get an image resolution score. For an

image with $n \times m$ pixels, the Brenner equation compares the level of gray transmission (G) between two points a few (in this case 2) pixels apart, giving a focus score, f.

$$f = \sum_m \sum_n \{G_{n,m} - G_{n+2,m}\}^2 \quad (8)$$

The focus depth with the highest score was saved as the final image capture. All final image captures were sequenced into an animation using ImageJ (National Institutes of Health, Bethesda, MD).

3 Results

3.1 One-Sided mPADs

In total, five (5) one-sided mPADs survived the preparation process and were able to be measured in the confocal microscope, three with 3.0 µm posts and two with 3.5 µm posts. The experiment ran for nearly eight hours before the imaging software crashed during the 97th capture sequence. The processed images revealed two (2) single-sided mPADs devices contained evidence of functional cell adhesion to the post tops.

Table 11: Summarized observations for single-sided mPADs experiment

Device	Post Diameter (µm)	Notes
#1	3.0	The mPADs coverslip became detached and floated freely in the well. **Inconclusive.**

#2	3.0	Cells visibly adhered the posts and to the post-height side walls. Cell movement along the top of the posts observable from t=335 min to t=480 min
#3	3.0	Possible partial cell adhesion visible for the duration of the experiment but no fully-spread and locomotive cells like in #2.
#4	3.5	Too much floating debris to discern cellular activity on the micropost surface. **Inconclusive.**
#5	3.5	Too much floating debris to discern cellular activity on the micropost surface. **Inconclusive.**

Device #2, most interestingly, clearly showed a cells locomoting on top of the microposts at speeds ranging from approximately 0.5 to 4.0 μm per minute. Figure 21 shows the bright field image (left), FITC fluorescent image (middle) and TRITC fluorescent image (right) of four cells adhered to the microposts at 375 minutes into the experiment. The RhoFN stamped on the microposts did not appear to result in significant labeling of the post tops themselves. Some scattered micropost tops were still brightly illuminated under the TRITC filter. Coincidentally, the post tops can still be visualized using the bright field and FITC filter. The movement seen in the animation is demonstrated in Figure 22, which compares a region of the bright field capture at 375 minutes to the same region 20 minutes later. The approximate initial cell shapes are highlighted in yellow and the final migrated shapes in blue for visibility. In general these

cells appeared to align parallel to one another along the micropost geometry and migrate in along that parallel axis. The cell shape resembles the native spread shape of an HUASMC on a two-dimensional surface.

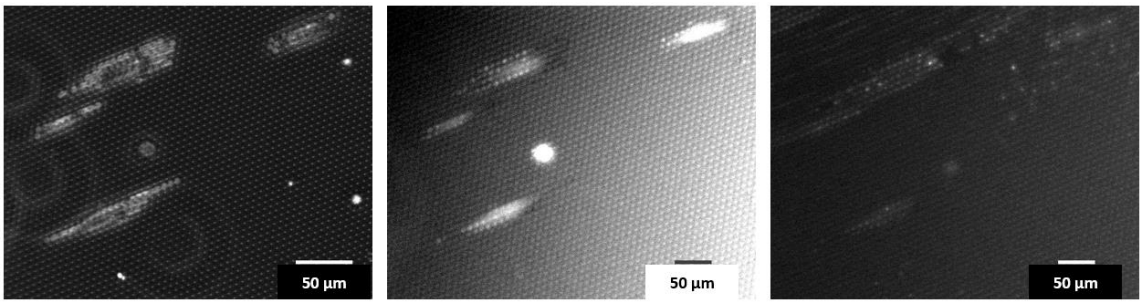

Figure 21: Still image of cells under bright field (left), FITC (center) and TRITC (right)

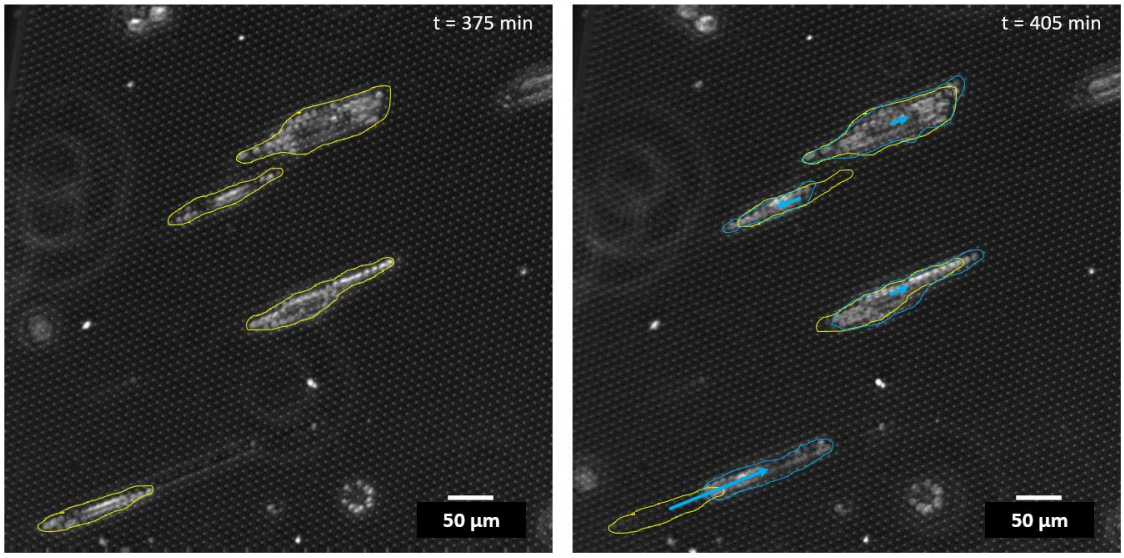

Figure 22: Movement of four cells in a 20-minute span (original position in yellow, new position in blue)

Additionally, some cells appeared to adhere to the posts, as evidenced by their synchronous movement with the mPADs device itself drifting in frame, but not fully-spread and motile as seen in Figure 23. These cells appeared more compact and circular in shape.

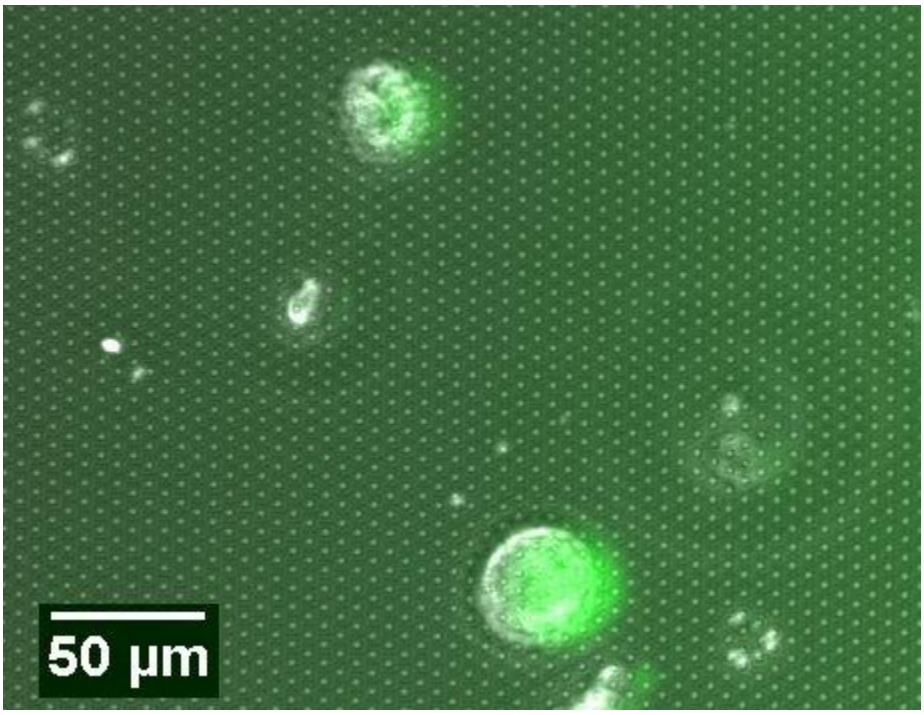

Figure 23: Adhered non-spread cells on single-sided mPADs

3.2 Two-Sided mPADs Sandwiches

In total, five (5) two-sided mPADs survived the preparation process and were able to be measured in the confocal microscope, three sets with 3.0 µm posts and two sets with 3.5 µm posts. Three different spacings were also used using the film preparation described in section 2.3.3.1 at 4000 RPM (10 µm), 5000 RPM (7 µm), and 6000 RPM (6

μm). One of each spacings were observed for the 3.0-μm post sandwiches and the 10- and 7-μm spacings were used in the case of the two 3.5-μm post sandwiches. In all five cases, cells were seeded originally to the bottom mPADs followed by placing the top mPADs device to form the sandwich. None of the 5 sandwiches revealed any clearly discernable cell adhesion to the top mPADs posts, the imaging is unclear and bottom-to-top adhesion may still have occurred in a limited capacity. The microscopy imaging of the two-sided devices suffered the same perils of the one-sided devices, namely difficulty keeping the posts in-focus and, to a lesser extent, keeping the devices themselves stationary in the 6-wells over the duration of the experiment.

Table 12 Summarized observations for two-sided mPADs experiment

Device	Post Diameter (μm)	Gap Spacing (μm)	Notes
#6	3.0	10	*Top mPADs:* Some cells are seen moving, but none in focus to certify attachment. **Inconclusive.** *Bottom mPADs:* One cell appears adhered to posts around t=225 min when it appears to either divide or otherwise start moving about half its mass away from the surface

#7	3.0	7	*Top mPADs:* Several cells in frame, but none are in focus. One appears adhered to something, but the image is not sufficiently focused to say if it is on microposts. **Inconclusive.** *Bottom mPADs:* Several cells in frame, but none are in focus. One appears adhered to something, but the image is not sufficiently focused to say if it is on microposts.
#8	3.0	6	Top mPADs: No cells in focus for duration. Bottom mPADs: This has the strongest signal on the TRITC filter. A few small cells appear attached to posts and moving around.
#9	3.5	10	Top mPADs: No cells in focus for duration. Bottom mPADs: Two cells appear in frame, one possibly adhered to posts

			Top mPADs: One almost comes into focus on upper center of the frame around t=30 minutes. **Inconclusive.**
#10	3.5	7	Bottom mPADs: Multiple cells are in frame, two small cells possibly adhered to the posts.

Figure 24-Figure 28 show some still images at interesting times on both the top and bottom mPADs. It is possible, though unverifiable that a cell might have bridged the gap from the bottom to the top of the mPADs due to the failure to focus on the post tops throughout the experiment. Notably, although cells can be seen adhered to the mPADs surface on the bottom devices, the elongated shape and migration seen in Figure 22 is not duplicated in the sandwich arrangement. All adherent cells appeared relatively compact and not spread over dozens of posts as in the single-sided experiment.

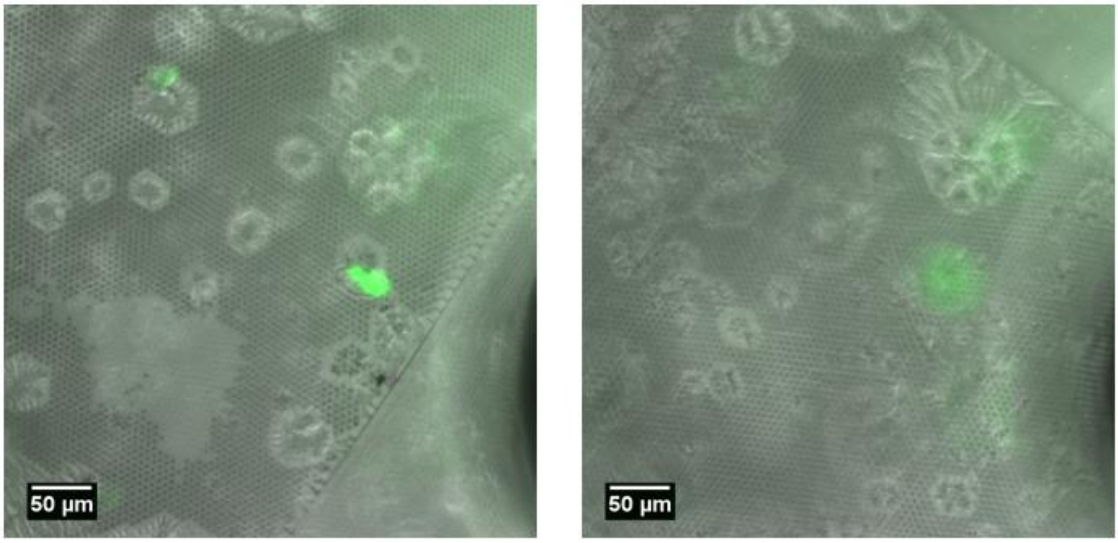

Figure 24: Two-sided mPADs device #6; bottom (left) and top (right) mPADs.

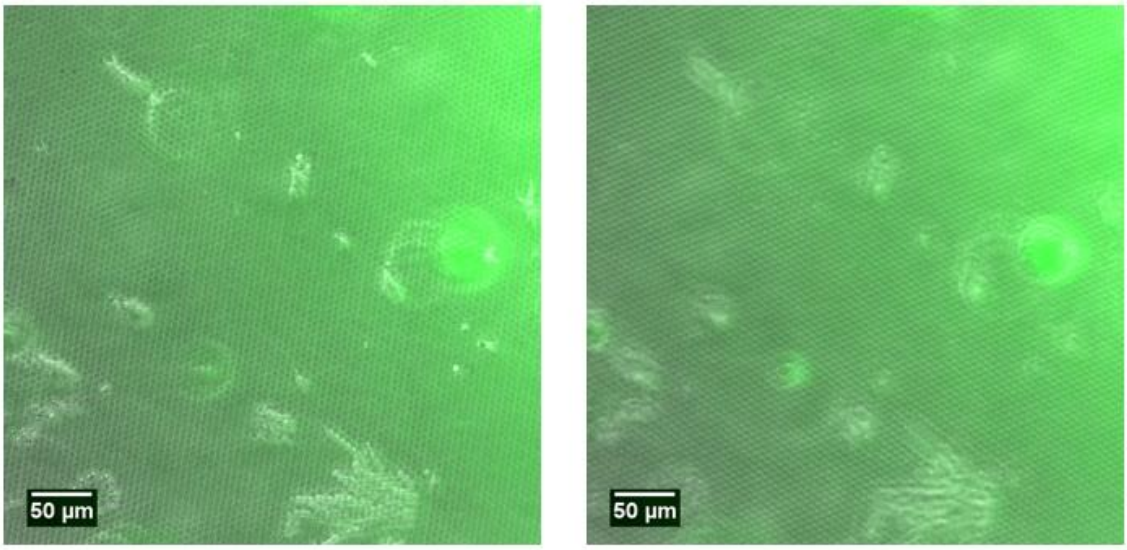

Figure 25: Two-sided mPADs device #7; bottom (left) and top (right) mPADs.

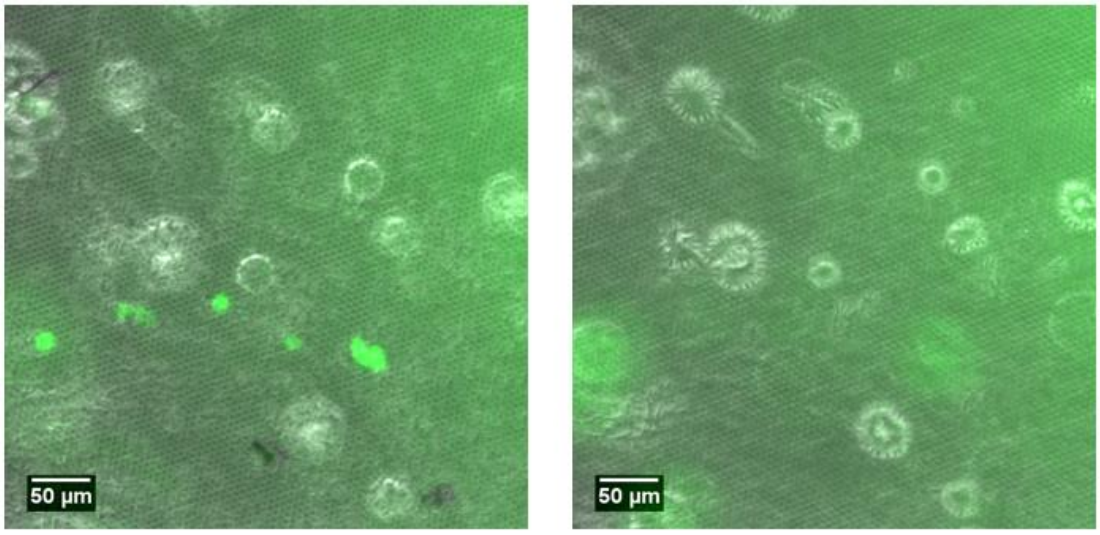

Figure 26: Two-sided mPADs device #8; bottom (left) and top (right) mPADs.

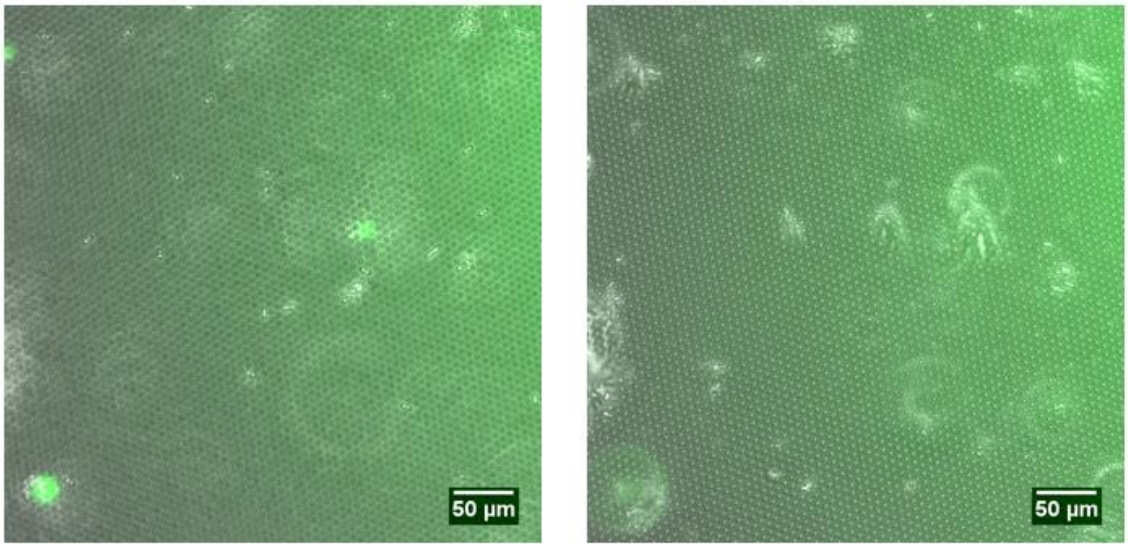

Figure 27: Two-sided mPADs device #9; bottom (left) and top (right) mPADs.

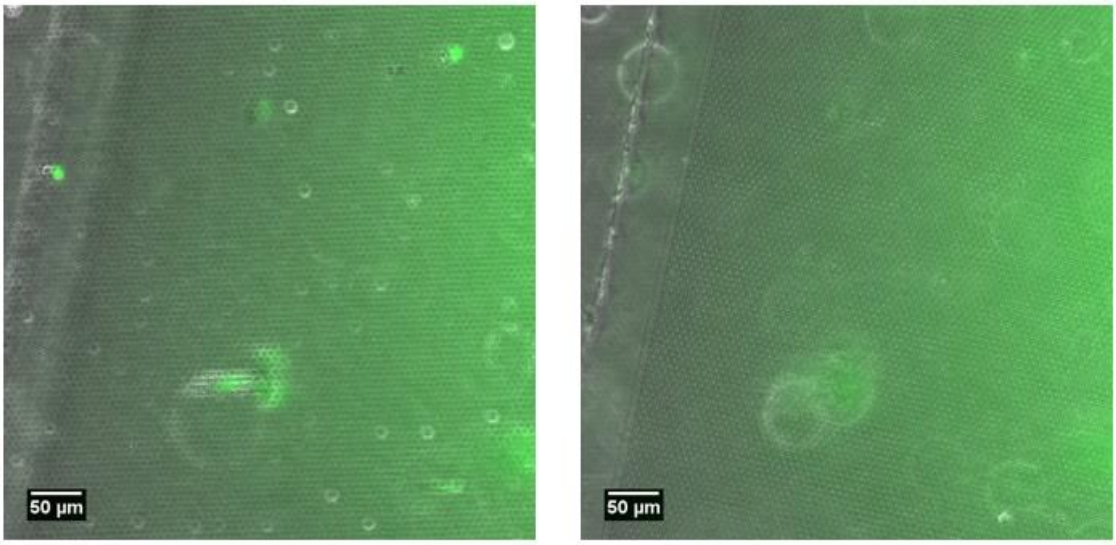

Figure 28: Two-sided mPADs device #10; bottom (left) and top (right) mPADs.

One other cell behavior noted on the two-sided mPADs sandwiches was an "anchored swinging" behavior. On the bottom mPADs of devices #6, #8, and #10, a cell could be seen at one end adhered, or at least not moving with respect to the microposts, while at the opposite end moving relatively quickly. Figure 29-Figure 31 show these cells and their movements in one 5-minute window.

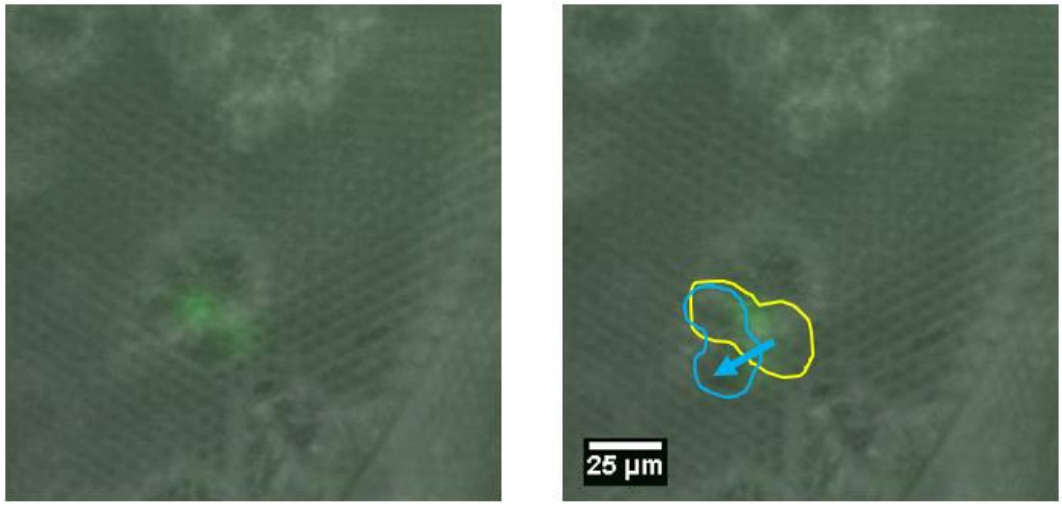

Figure 29: Rapid anchored swinging movement seen on mPADs device #6.

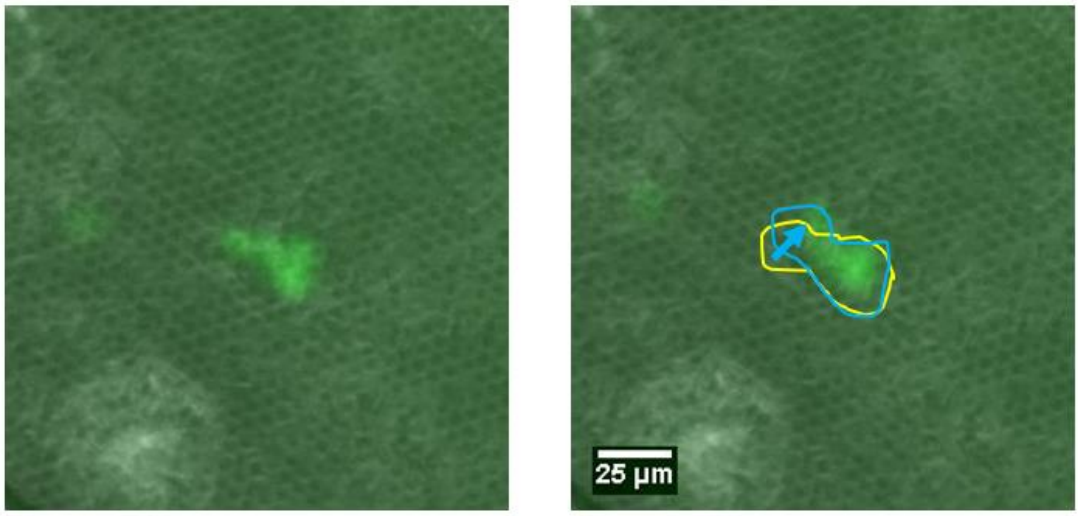

Figure 30: Rapid anchored swinging movement seen on mPADs device #8.

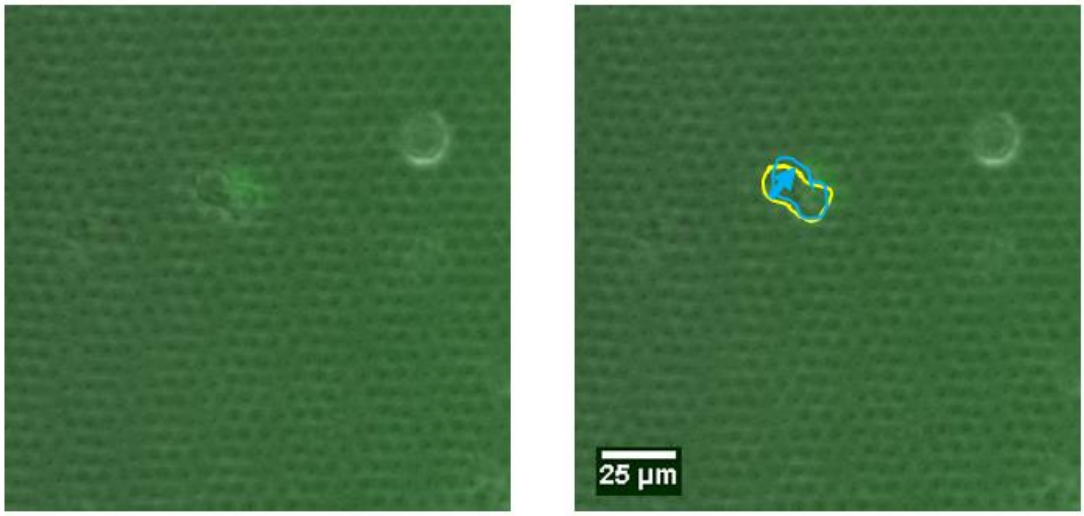

Figure 31: Rapid anchored swinging movement seen on mPADs device #10.

Other than the cells themselves, there are other objects to note on the microscope imaging. There are multiple areas where the micropost structure appears damaged or malformed. The mPADs were inspected prior to use in the experiment and selected for their large areas of flawless micropost arrays. Imaging was limited to areas where both the top and bottom mPADs had both of the following:

1) Living cells present with CellTracker Green
2) Overlapping regions of "good" micropost arrays to image

In several cases, in order to image living cells, regions with less-than-perfect (e.g., missing or collapsed posts) micropost structures had to be utilized.

Not clearly seen in any one still image are suspended cells highlighted with CellTracker Green floating around many of the images out-of-focus. It was clear that

many of the seeded cells never spread onto the mPADs themselves and continued to float round the media during the experiment. Also, some debris are seen (Figure 32). The source of the debris is unclear, but possible culprits are dead cell material (no CellTracker Green signal can be detected), air bubbles, or another foreign contaminant on the mPADs themselves.

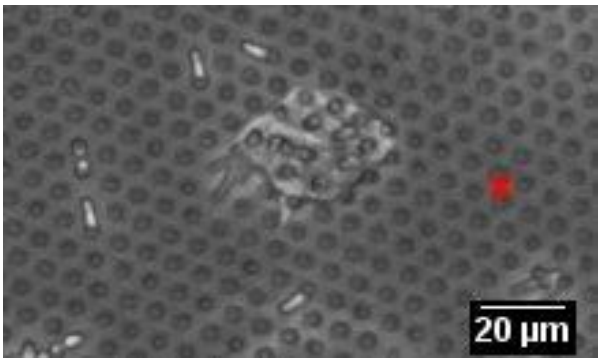

Figure 32: Unidentified debris

4 Discussion

4.1 Comments on Results

The experimental results obtained in section 3 do not clearly demonstrate the efficacy of pseudo-3D mPADs devices to measure cell behavior in a non-spread environment. That is not to entirely say that the experiment was completely uninteresting. The impact of adding a capping mPADs device to the original single-surfaced apparatus did result in differing cellular behaviors.

The primary difference observed is the manner of cell attachment and spreading observed. Fully spread cells were identified on the single-sided mPADs. These were readily identifiable; the HUASMCs resembled their natural spread state when imaged on a flat surface, such as a T75 cell culture flask. No such spreading, however, was seen in the cells observed in the two-sided mPADs sandwiches. In the pseudo-3D devices, cells only appeared compact and round, even when adhered. It is difficult to conclude if this is a coincidence or the result of the steric interference from the top mPADs.

Additionally, there were three observed cases of a cell appearing to "reach" around the intra-post space in the two-sided devices. These cells were polarized, with one end of the cell was fixed on the posts while the other was rapidly moving. This behavior was not observed on the single-sided experiments. Again, the significance of this observation is unclear.

4.2 Possible Failure Modes

Ultimately, the experiment described above failed to provide a firm acceptance or rejection of the hypothesis that a two-sided mPADs sandwich could be a useful tool in observing and modulating cellular behavior in a pseudo-3D environment. Looking back, there are several possible failure points in the manufacture and assembly of the mPADs that could have muddled the results.

4.2.1 Low Throughput of mPADs

One of the primary concerns in preparation for the experiment was obtaining sufficient mPADs devices. After the master silicon wafer was fabricated and silanized, the subsequent steps required several days of work to get to a final product. The immediate first steps in the process would require three days and already resulted in a failure rate. This took one day to mix and cure a negative mold from the wafer, one day to cut and silanized individual negative molds, and one day to create positive mPADs molds on coverslips. At this point, the devices were inspected to see if they were either successfully fabricated or could be recovered with critical point drying. As discussed in section [2.4.2 ii], only the 3.0- and 3.5-μm diameter microposts were used as they were the most abundant. In fact, a 2.0-μm diameter micropost device never survived the initial first three days and, of the four 2.5-μm diameter micropost device molds on the negative mold design, only one device could seldomly be recovered. Although multiple batches of mPADs could be staggered and manufactured concurrently, it still took 3 days to produce only four to eight successful mPADs for the remaining steps.

When sufficient 3.0- and 3.5-μm diameter mPADs were fabricated, *then* a trip could be made to process a batch in the critical point dryer and the number of surviving mPADs could be assessed. The number of mPADs whose array structures could be recovered by CPD was always less than 100 percent. Finally, mPADs which survived the manufacturing process to this point were at risk of handling failures (e.g. broken coverslips, damage to the PSMS surface, etc.) during the process of adding the sidewall. In sum, it often took as many as 4-5 weeks just to obtain sufficient quantities of mPADs with large regions of flawless microposts in order to run a single experiment. As a result,

the amount of titration and calibration required to improve the likelihood of success on the day of any given experiment was certainly hindered.

4.2.2 Final Assembly Concerns

During the course of the experiment itself there were several failure points and potential concerns which may have doomed final result. The most obvious issue was the failure of the devices to "stay put" inside the six well during the course of the experiment. The six well sat in a moving microscope stage and each device was tacked down using some silicone gel. While the gel held some devices in place successful, after cell media was added to the wells the gel was susceptible to wetting and release from the bottom of the plastic well leaving the mPADs to float and drift out of focus.

Another concern was the application of RhoFN to mark the tops of the posts. There TRITC filter did not pick up much, if any signal of the fluorescent Rhodamine except in a few cases where a small region of posts were brightly illuminated. For instance, Figure 33 shows the bottom mPADs in device #8 with the brightness enhanced. This shows the TRITC filter finding small discrete regions of posts illuminated with RhoFN, but the field of posts is largely unmarked by fluorescence. It is possible that the FN + RhoFN preparation in section (2.4.2.1) failed to properly suspend RhoFN in a high enough concentration to evenly stamp the post tops. Alternatively, the stamping

procedure could have also failed. The arrays of posts in the mPADs used were almost never completely flawless across the entire stamping surface. The mPADs were selected for having large regions of flawless post arrays, but they almost always had other post array regions that had totally collapsed or were malformed. The imperfection of the micropost arrays could have prevented a clean, even stamp application to the top of the posts.

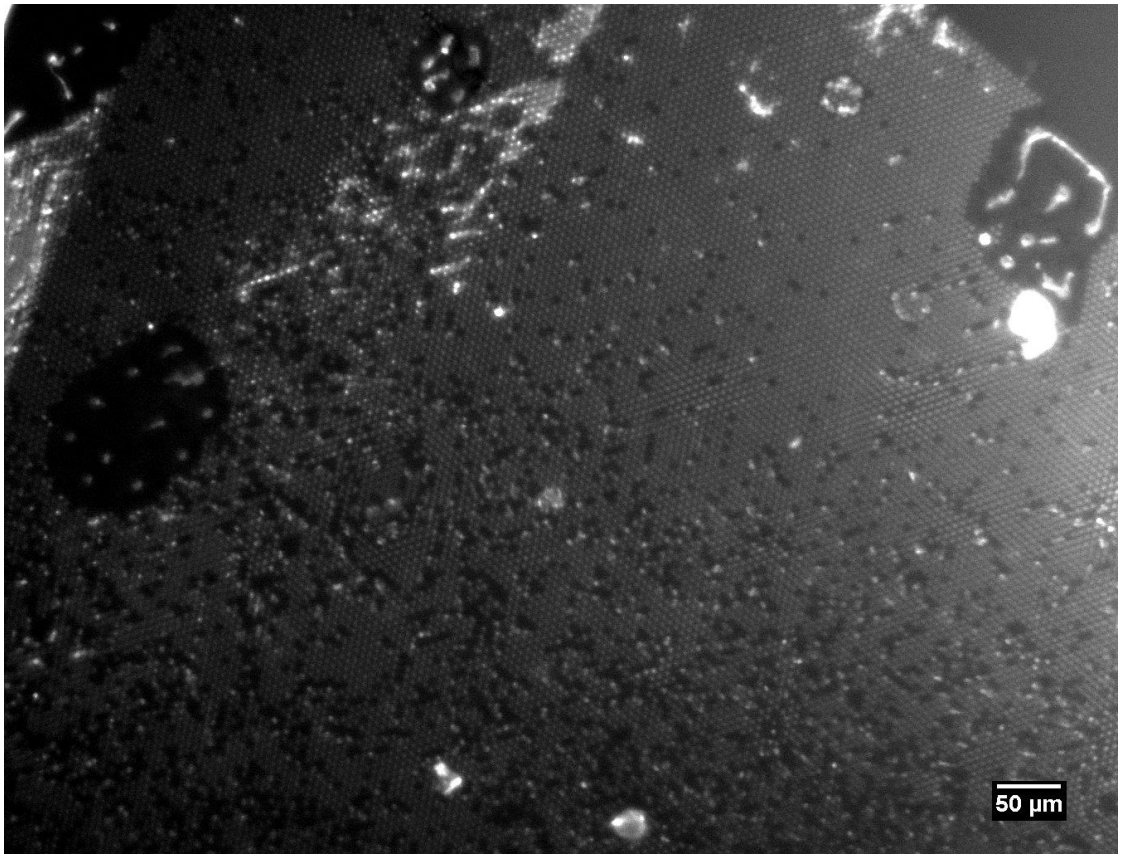

Figure 33: FITC Image on bottom device of mPADs system #8

4.2.3 Cellular Behavior and Cytotoxicity

Another factor which could have affected the behavior of cells in the two-sided mPADs devices was the lack of media flow inside the mPADs sandwich. In all devices, one- and two-sided, the media in the six wells was orange (pH acidic) when retrieved the next morning. The HUAVSMC manufacturer recommends 1 mL media per 5 cm^2 when culturing cells. Obviously, the experimental condition is not intended to replicate cell culture in a T75 flask, but the volume of media contained inside the ~3 cm^2 two-sided mPADs apparatus is on the order of 2-3 µL, not mL. If the media is not actively flowing through the mPADs gap, the local nutrient density around the mPADs could be significantly impacted. Combine that with the relatively harsh conditions inside the confocal stage and it's possible that any changes in cell behavior between the one- and two-sided mPADs were entirely due to steric effects.

5 Conclusion and Future Considerations

This study attempted to create a novel device to measure and modulate cellular activity by applying mPADs in a pseudo-3D environment. A device design was successfully fabricated and characterized for such a use, but ultimately no clear evidence was captured to show that cells actively engaged both the top and bottom mPADs in the device as intended. Future study toward this goal might consider the many technical obstacles which prevented this design from succeeding. The concept of the device in this experiment ultimately relied heavily on human handling, introducing several possible errors and failure points into the final manufactured product. Utilizing technologies such as 3D printing or an expanded use of photolithography could aid in the throughput issues.

For instance, creating a second master silicon wafer which includes the mPADs spacer into the initial mold could eliminate this entire process step.

References

Abercrombie, M., Heaysman, J.E.M., and Pegrum, S.M. (1971). The locomotion of fibroblasts in culture: IV. Electron microscopy of the leading lamella. Exp. Cell Res. *67*, 359–367.

Amato, L., Keller, S.S., Heiskanen, A., Dimaki, M., Emnéus, J., Boisen, A., and Tenje, M. (2012). Fabrication of high-aspect ratio SU-8 micropillar arrays. Microelectron. Eng. *98*, 483–487.

Bhattacharya, S., Datta, A., Berg, J.M., and Gangopadhyay, S. (2005). Studies on surface wettability of poly(dimethyl) siloxane (PDMS) and glass under oxygen-plasma treatment and correlation with bond strength. J. Microelectromechanical Syst. *14*, 590–597.

Blanchoin, L., Boujemaa-Paterski, R., Sykes, C., and Plastino, J. (2014). Actin Dynamics, Architecture, and Mechanics in Cell Motility. Physiol. Rev. *94*, 235–263.

Brenner, J.F., Dew, B.S., Horton, J.B., King, T., Neurath, P.W., and Selles, W.D. (1976). An automated microscope for cytologic research a preliminary evaluation. J. Histochem. Cytochem. *24*, 100–111.

Cukierman, E., Pankov, R., Stevens, D.R., and Yamada, K.M. (2001). Taking cell-matrix adhesions to the third dimension. (Reports). Science *294*, 1708–1712.

Data, R. and (2019). Cardiovascular Devices Market to Reach USD 69.08 Billion by 2026 | Reports And Data.

Elliott, N.T., and Yuan, F. (2011). A Review of Three-Dimensional In Vitro Tissue Models for Drug Discovery and Transport Studies. J. Pharm. Sci. *100*, 59–74.

Faxon, D., Coats, W., and Currier, J. (1997). Remodeling of the coronary artery after vascular injury. Prog. Cardiovasc. Dis. *40*, 129–140.

Galbraith, C.G., and Sheetz, M.P. (1997). A Micromachined Device Provides a New Bend on Fibroblast Traction Forces. Proc. Natl. Acad. Sci. U. S. A. *94*, 9114–9118.

Galbraith, C.G., and Sheetz, M.P. (1998). Measuring Cellular Traction Forces with Micromachined Substrates. In Modern Optics, Electronics and High Precision Techniques in Cell Biology, G. Isenberg, ed. (Berlin, Heidelberg: Springer Berlin Heidelberg), pp. 195–210.

Georges, P., and Janmey, P. (2005). Invited Review Cell type-specific response to growth on soft materials. J. Appl. Physiol. *98*, 1547–1553.

Harris, A.K., Wild, P., and Stopak, D. (1980). Silicone Rubber Substrata: A New Wrinkle in the Study of Cell Locomotion. Science *208*, 177–179.

Higuchi, A., Sugiyama, K., Yoon, B.O., Sakurai, M., Hara, M., Sumita, M., Sugawara, S., and Shirai, T. (2003). Serum protein adsorption and platelet adhesion on pluronic^{TM}-adsorbed polysulfone membranes. Biomaterials *24*, 3235–3245.

J C Lötters (1997). The mechanical properties of the rubber elastic polymer polydimethylsiloxane for sensor applications. J. Micromechanics Microengineering *7*, 145–147.

Jothimuthu, P., Carroll, A., Bhagat, A.A.S., Lin, G., Mark, J.E., and Papautsky, I. (2009). Photodefinable pdms thin films for microfabrication applications. J. Micromechanics Microengineering *19*, 9.

Koschwanez, J.H., Carlson, R.H., and Meldrum, D.R. (2009). Thin PDMS Films Using Long Spin Times or Tert-Butyl Alcohol as a Solvent. PLoS ONE *4*.

Kristopher E. Kubow, and Alan Rick Horwitz (2010). Reducing background fluorescence reveals adhesions in 3D matrices. Nat. Cell Biol. *13*, 3–5; author reply 5-7.

Li, D., Wen, Z., Shang, Z., and She, Y. (2016). Thick SU8 microstructures prepared by broadband UV lithography and the applications in MEMS devices. Optoelectron. Lett. *12*, 182–187.

Li, S., Lao, J., Chen, B., Li, Y., Zhao, Y., Chu, J., Chen, K., Tsou, T.C., Peck, K., and Chien, S. (2002). Genomic analysis of smooth muscle cells in three-dimensional collagen matrix. Faseb J. *16*, 97–979.

Maazouz, Y., Montufar, E.B., Malbert, J., Espanol, M., and Ginebra, M.-P. (2017). Self-hardening and thermoresponsive alpha tricalcium phosphate/pluronic pastes. Acta Biomater. *49*, 563–574.

MacKintosh, F.C., Käs, J., and Janmey, P.A. (1995). Elasticity of Semiflexible Biopolymer Networks. Phys. Rev. Lett. *75*, 4425–4428.

Madou, M.J. (2002). Fundamentals of microfabrication: the science of miniaturization (Boca Raton: CRC Press).

Merkle, V.M., Tran, P.L., Hutchinson, M., Ammann, K.R., DeCook, K., Wu, X., and Slepian, M.J. (2015). Core–shell PVA/gelatin electrospun nanofibers promote human umbilical vein endothelial cell and smooth muscle cell proliferation and migration. Acta Biomater. *27*, 77–87.

Michael T Yang, Jianping Fu, Yang-Kao Wang, Ravi A Desai, and Christopher S Chen (2011). Assaying stem cell mechanobiology on microfabricated elastomeric substrates with geometrically modulated rigidity. Nat. Protoc. *6*, 187–213.

Müller, U., Timpe, H.-J., and Neuenfeld, J. (1991). Photocrosslinking of silicones—5. Photo-induced polymerization of silicone with pendant acrylate groups in the presence of oxygen. Eur. Polym. J. *27*, 621–625.

Müller, U., Jockusch, S., and Timpe, H.-J. (1992). Photocrosslinking of silicones. VI. Photocrosslinking kinetics of silicone acrylates and methacrylates. J. Polym. Sci. Part Polym. Chem. *30*, 2755–2764.

Özçam, A.E., Efimenko, K., and Genzer, J. (2014). Effect of ultraviolet/ozone treatment on the surface and bulk properties of poly(dimethyl siloxane) and poly(vinylmethyl siloxane) networks. Polymer *55*, 3107–3119.

Pelham, R.J., and Wang, Y.L. (1999). High resolution detection of mechanical forces exerted by locomoting fibroblasts on the substrate. Mol. Biol. Cell *10*, 935–945.

Pollard, T.D., Earnshaw, W.C., Lippincott-Schwartz, J., and Johnson, G.T. (2017). Cellular Adhesion. In Cell Biology, (Philadelphia, PA: Elsevier), pp. 525–541.

Ridley, A.J. (2003). Cell Migration: Integrating Signals from Front to Back. Sci. Am. Assoc. Adv. Sci. *302*, 1704–1709.

Schwartz, M., and Chen, C. (2013). Deconstructing Dimensionality. Science *339*, 402–404.

Sniadecki, N.J., and Chen, C.S. (2007). Microfabricated Silicone Elastomeric Post Arrays for Measuring Traction Forces of Adherent Cells. Methods Cell Biol. *83*, 313–328.

Fraley, S.I., Yunfeng Feng, Ranjini Krishnamurthy, Dong-Hwee Kim, Alfredo Celedon, Gregory D. Longmore, and Denis Wirtz (2010). A distinctive role for focal adhesion proteins in three-dimensional cell motility. Nat. Cell Biol. *12*, 598–604.

Tan, J.L., Tien, J., Pirone, D.M., Gray, D.S., Bhadriraju, K., and Chen, C.S. (2003). Cells lying on a bed of microneedles: an approach to isolate mechanical force.(Abstract). Proc. Natl. Acad. Sci. U. S. *100*, 1484–1489.

Tolde, O., Rösel, D., Janoštiak, R., Veselý, P., and Brábek, J. (2012). Dynamics and morphology of focal adhesions in complex 3D environment. Folia Biol. (Praha) *58*, 177–184.

Tsougeni, K., Tserepi, A., and Gogolides, E. (2007). Photosensitive poly(dimethylsiloxane) materials for microfluidic applications. Microelectron. Eng. *84*, 1104–1108.

Virani, S.S., Alonso, A., Benjamin, E.J., Bittencourt, M.S., Callaway, C.W., Carson, A.P., Chamberlain, A.M., Chang, A.R., Cheng, S., Delling, F.N., et al. (2020). Heart

Disease and Stroke Statistics—2020 Update: A Report From the American Heart Association. Circ. N. Y. N *141*, e139–e151.

Wells, C.M. (2011). Cell Migration Developmental Methods and Protocols (Totowa, NJ: Humana Press).

Wozniak, M.A., Desai, R., Solski, P.A., Der, C.J., and Keely, P.J. (2003). ROCK-generated contractility regulates breast epithelial cell differentiation in response to the physical properties of a three-dimensional collagen matrix. J. Cell Biol. *163*, 583–595.

Ying Mei, Krishanu Saha, Said R. Bogatyrev, Jing Yang, Andrew L. Hook, Z. Ilke Kalcioglu, Seung-Woo Cho, Maisam Mitalipova, Neena Pyzocha, Fredrick Rojas, et al. (2010). Combinatorial development of biomaterials for clonal growth of human pluripotent stem cells. Nat. Mater. *9*, 768–778.

Zaidel-Bar, R., Itzkovitz, S., Ma'ayan, A., Iyengar, R., and Geiger, B. (2007). Functional atlas of the integrin adhesome. Nat. Cell Biol. *9*, 858–867.

Zhang, W.Y., Ferguson, G.S., and Tatic-Lucic, S. (2004). Elastomer-supported cold welding for room temperature wafer-level bonding. In 17th IEEE International Conference on Micro Electro Mechanical Systems. Maastricht MEMS 2004 Technical Digest, pp. 741–744.

Zhao, Y., Lim, C.C., Sawyer, D.B., Liao, R., and Zhang, X. (2005). Cellular force measurements using single-spaced polymeric microstructures: isolating cells from base substrate. J. Micromechanics Microengineering *15*, 1649–1656.

Zhou, X., Rowe, R.G., Hiraoka, N., George, J.P., Wirtz, D., Mosher, D.F., Virtanen, I., Chernousov, M.A., and Weiss, S.J. (2008). Fibronectin fibrillogenesis regulates three-dimensional neovessel formation. Genes Dev. *22*, 1231–1243.

Fisherbrand Cover Glasses: Circles - Microscopes, Slides and Coverslips, Coverslips.

Appendix: MATLAB Script for Image Processing

```
%%This .m file will read a series of tiff images stacks and indicate the
%%most in-focus photo on each stack.

%7/28 images have 11 slices per tif and 96 full time increments
%7/29 images have 6 slices per tif and 57 full time increments

clear all;

test_image_prefixes = {{ 'HUAVSMC_P6_1Side__w1BF CCD_s1_t'; %Create array
with all file prefixes
                'HUAVSMC_P6_1Side__w1BF CCD_s2_t';
                'HUAVSMC_P6_1Side__w1BF CCD_s3_t';
                'HUAVSMC_P6_1Side__w1BF CCD_s4_t';
                'HUAVSMC_P6_1Side__w1BF CCD_s5_t';
                'HUAVSMC_P6_1Side__w2FITC CCD_s1_t';
                'HUAVSMC_P6_1Side__w2FITC CCD_s2_t';
                'HUAVSMC_P6_1Side__w2FITC CCD_s3_t';
                'HUAVSMC_P6_1Side__w2FITC CCD_s4_t';
                'HUAVSMC_P6_1Side__w2FITC CCD_s5_t';
                'HUAVSMC_P6_1Side__w3TRITC CCD_s1_t';
```

'HUAVSMC_P6_1Side__w3TRITC CCD_s2_t';

'HUAVSMC_P6_1Side__w3TRITC CCD_s3_t';

'HUAVSMC_P6_1Side__w3TRITC CCD_s4_t';

'HUAVSMC_P6_1Side__w3TRITC CCD_s5_t'}

{'HUAVSMC_P6_2Side__w1BF CCD_s1_t';

'HUAVSMC_P6_2Side__w1BF CCD_s2_t';

'HUAVSMC_P6_2Side__w1BF CCD_s3_t';

'HUAVSMC_P6_2Side__w1BF CCD_s4_t';

'HUAVSMC_P6_2Side__w1BF CCD_s5_t';

'HUAVSMC_P6_2Side__w1BF CCD_s6_t';

'HUAVSMC_P6_2Side__w1BF CCD_s7_t';

'HUAVSMC_P6_2Side__w1BF CCD_s8_t';

'HUAVSMC_P6_2Side__w1BF CCD_s9_t';

'HUAVSMC_P6_2Side__w1BF CCD_s10_t';

'HUAVSMC_P6_2Side__w1BF CCD_s11_t';

'HUAVSMC_P6_2Side__w2FITC CCD_s1_t';

'HUAVSMC_P6_2Side__w2FITC CCD_s2_t';

'HUAVSMC_P6_2Side__w2FITC CCD_s3_t';

'HUAVSMC_P6_2Side__w2FITC CCD_s4_t';

'HUAVSMC_P6_2Side__w2FITC CCD_s5_t';

'HUAVSMC_P6_2Side__w2FITC CCD_s6_t';

'HUAVSMC_P6_2Side__w2FITC CCD_s7_t';

```
                'HUAVSMC_P6_2Side__w2FITC CCD_s8_t';
                'HUAVSMC_P6_2Side__w2FITC CCD_s9_t';
                'HUAVSMC_P6_2Side__w2FITC CCD_s10_t';
                'HUAVSMC_P6_2Side__w2FITC CCD_s11_t';
                'HUAVSMC_P6_2Side__w3TRITC CCD_s1_t';
                'HUAVSMC_P6_2Side__w3TRITC CCD_s2_t';
                'HUAVSMC_P6_2Side__w3TRITC CCD_s3_t';
                'HUAVSMC_P6_2Side__w3TRITC CCD_s4_t';
                'HUAVSMC_P6_2Side__w3TRITC CCD_s5_t';
                'HUAVSMC_P6_2Side__w3TRITC CCD_s6_t';
                'HUAVSMC_P6_2Side__w3TRITC CCD_s7_t';
                'HUAVSMC_P6_2Side__w3TRITC CCD_s8_t';
                'HUAVSMC_P6_2Side__w3TRITC CCD_s9_t';
                'HUAVSMC_P6_2Side__w3TRITC CCD_s10_t';
                'HUAVSMC_P6_2Side__w3TRITC CCD_s11_t'}};


directory =    ['D:\\Jeff\\Confocal Images\\20180728'; %ID Directories
            'D:\\Jeff\\Confocal Images\\20180729'];


experiment_days = [ '28-JUL';
                '29-JUL']; %text indicator of which experiment day is in question
```

```
time_stamps = [96 57]; % number of completed increments per day

num_slice = [11 6]; % number of slices per tif file per day


progress_count = 0; %iterator


for day = 1:2 %two days of experients


BEST_ONES = zeros(length(test_image_prefixes{day}),time_stamps(day)); %Saves the
"best" file slice


write_directory = 'D:\\Jeff\\Confocal Images\\Jul 28 and 29 expermients processed';
%establishes directory
write_filename = sprintf('most_in_focus_%s.txt',experiment_days(day,:)); % establishes
filename


write_file = fullfile(write_directory,write_filename); %combines directory and filename
writer = fopen(write_file,'wt'); % writes file



for site = 1:length(test_image_prefixes{day}) %for each imaging site from the
microscope


    Site_prefix = char(test_image_prefixes{day}(site,:));%read in filename
```

```
    Site_label = Site_prefix(1:end-2) + "\n"; %truncate the trailing characters, instead
begin a new line
    fprintf(writer, Site_label); %print the site to a text file
    gif_file = Site_prefix(1:end-2)+".gif";  %prepare gif filename

for t_mark = 1:time_stamps(day) %for each time increment

    best_res = 0; % reset best resolution score

    for slice = 1:num_slice(day) %for each slice

        filename = [char(test_image_prefixes{day}(site)), num2str(t_mark), '.tif'];%read file

        this_tiff = fullfile(directory(day,:),filename); %combine directory and filename

        object = Tiff(this_tiff,'r'); %Create a TIFF object

        imagedata = imread(this_tiff,slice)*8; %read the image data

        % Run each image through the Brenner equation to get a resolution
        % score, FM
        [M,N] = size(imagedata);
        DH = zeros(M,N);
```

```
    DV = zeros(M,N);
    DV(1:M-2,:) = imagedata(3:end,:)-imagedata(1:end-2,:);
    DV = DV.*DV;
    DH(:,1:N-2) = imagedata(:,3:end)-imagedata(:,1:end-2);
    DH=DH.*DH;
    FM = DV + DH;
    FM = sqrt(mean2(FM)) * M * N / (M * N - 4);

    %if FM is the best score yet, make this slice the new "best_res"
    if FM > best_res

        best_res = FM;
        BEST_ONES(site,t_mark) = slice + ((t_mark - 1)*num_slice(day));
        best_slice = slice;

    end %end if FM

end %end for slice

if t_mark == time_stamps(day) %write the resulting best image slice followed

    fprintf(writer,'%d',BEST_ONES(site,t_mark));
```

```
    else

        fprintf(writer,'%d, ',BEST_ONES(site,t_mark)); %follow with a comma if not the
final time stamp

    end %end if t_mark

    %save only the most-in-focus images to a new directory.
    bestslicefile = [char(test_image_prefixes{day}(site)), num2str(t_mark), '.tif'];

    bestslicetiff = fullfile(directory(day,:),bestslicefile);

    u16_data = imread(bestslicetiff,best_slice);

    best_filename = sprintf('in_focus_%s%i.tif',Site_prefix,t_mark);

    best_write_file = fullfile(write_directory,best_filename);

    imwrite(u16_data, best_write_file);

end %end for t_mark

    %Progres Tracker
```

```
    progress_count = progress_count + 1;

    progress = (progress_count/48)*100;

    display(sprintf('%.2f%% complete',progress));

    fprintf(writer,'\n');

end %end for each image

fclose(writer);

end %end for each day


%notify completion
load handel
sound(y,Fs)
```